energies

MDPI

Article

Analysis and Evaluation of the Operating Profile of a DC Inverter in a PV Plant

Silvia Baeva [1], Ivelina Hinova [2] and Plamen Stanchev [3,4,*]

[1] Department of Mathematical Modelling and Numerical Methods, Faculty of Applied Mathematics and Informatics, Technical University of Sofia, 1000 Sofia, Bulgaria; sbaeva@tu-sofia.bg
[2] Department of Management and Business Information Systems, Faculty of Management, Technical University of Sofia, 1000 Sofia, Bulgaria; ihinova@tu-sofia.bg
[3] CoE "National Center of Mechatronics and Clean Technologies", 1000 Sofia, Bulgaria
[4] Department of Information Technology in Industry, Faculty of Computer Systems and Technologies, Technical University of Sofia, 1000 Sofia, Bulgaria
* Correspondence: p.stanchev@tu-sofia.bg

Abstract

The inverter is the key element that converts the intermittent DC power of the PV array into a quality AC flow to the grid and simultaneously performs functions such as power factor control, reactive services, and grid code compliance. Therefore, the detailed operating profile of the inverter, how the power, dynamics, power quality, and efficiency evolve over time, is critical for both the scientific understanding of the system and the daily operation (O&M). Monitoring only aggregated energy indicators or single KPIs (e.g., PR) is often insufficient: it does not distinguish weather-related variations from technical limitations (clipping, curtailment), does not show dynamic loads (ramp rate), and does not provide confidence in the quality of the injected energy (PF, P–Q behavior). These deficiencies motivate research that simultaneously covers the physical side of the conversion, the operational dynamics, and the climatic reference of the resource. The analysis covers the window of 25 January–15 April 2025 (winter→spring). Due to the pronounced seasonality of the solar resource and temperature regime, all quantitative results and conclusions regarding efficiency, dynamics, clipping, and degradation are valid only for this window; generalizations to other seasons require additional data. In the next stage, we will add $\geq$12 months of data and perform a comparable seasonal analysis. Full specifications of the measuring equipment (DC/AC current/voltage, clock synchronization, separate high-frequency PQ-logger) and quantitative uncertainty estimates, including distribution to key indicators (η, PR, THD, I_{DC}), are presented. The PVGIS per-kWp climate reference is anchored to the nameplate DC peak and cross-checked against percentile scaling; $a \pm \varepsilon$ scale error shifts PR by ε and changes ΔE proportionally only on hours with $\hat{P} > P$. The capacity for the climate reference (PVGIS per-kWp) is calibrated to the tabulated DC peak power C_{cert} and is cross-validated using a percentile scale ($Q_{0.99}$).

Keywords: photovoltaic systems; DC/AC inverter; inverter operating profile; power quality assessment; inverter efficiency; SCADA monitoring; climate-normalized performance ratio

check for updates

Academic Editor: Hervé Morel

Received: 21 October 2025
Revised: 12 November 2025
Accepted: 25 November 2025
Published: 30 November 2025

Citation: Baeva, S.; Hinova, I.; Stanchev, P. Analysis and Evaluation of the Operating Profile of a DC Inverter in a PV Plant. *Energies* **2025**, *18*, 6306. https://doi.org/10.3390/en18236306

Copyright: © 2025 by the authors. Licensee MDPI, Basel, Switzerland. This article is an open access article distributed under the terms and conditions of the Creative Commons Attribution (CC BY) license (https://creativecommons.org/licenses/by/4.0/).

1. Introduction

Photovoltaic (PV) systems are a leading component in the transition to a low-carbon energy system and sustainable power generation. Their gradual penetration into the power grid, both in large-scale ground-based parks and in decentralized rooftop installations,

places increasingly high demands on the reliability, efficiency, and controllability of their components. Among them, the DC/AC inverter plays a central role, as it is not only a converter of electrical energy from direct to alternating current but also actively participates in the network behavior of the installation, including through power factor management, reactive services, ramp-rate limitations, and compatibility with standards such as IEEE 1547, EN 50530, and Network Code RfG.

Traditional approaches to PV system evaluation rely primarily on aggregated energy metrics, such as the power output over time, capacity factor, or performance ratio. These metrics do not adequately capture the dynamic processes occurring in the system in real time despite their usefulness in long-term performance evaluation. Such processes include power limitations due to inverter limits, partial shading losses, unstable MPPT behavior, reactive interference, or short-term shutdowns and restarts.

Furthermore, aggregate indicators do not allow a reliable distinction between losses caused by adverse climatic conditions (e.g., low light or high temperature) and those resulting from technical reasons, such as configuration errors, component degradation, or inverter operation errors. This creates a need to introduce a deeper and structured approach to inverter operation analysis that takes into account both temporal changes in system behavior and the climatic context.

In that sense, this study introduces and applies the concept of the "inverter operating profile", which represents the time trajectory of the main electrical and energy parameters, including active and reactive power, voltages and currents on the DC and AC sides, power factor, conversion efficiency, ramp rate, as well as indicators related to power quality, such as harmonic distortion and frequency stability.

The construction of such a working profile aims to provide a more detailed and quantitative assessment of the inverter's condition and behavior in real-world operation. For this purpose, real operational data recorded by the SCADA system of a Photovoltaic Power Plant in Bulgaria, with a high time resolution (5 min interval), covering a significant period of the winter and spring season, are used. The analysis in this work is explicitly limited to the window of 25 January 2025–15 April 2025 (local time), i.e., the winter→spring transition. This is sufficient for demonstration and verification of the methodology, but is not a basis for annual conclusions about PR, clipping, and degradation. The data include complete information from both the DC side (voltage, current, instantaneous power) and the AC side (output active and reactive power, $\cos\varphi$, efficiency), and are combined with climatic reference data provided by open sources such as PVGIS, PECD, and NASA POWER.

The methodology proposed in this study is based on an integrated approach that combines several basic steps:

1. Physically based recovery of the instantaneous active power, which takes into account the real efficiency of the inverter at any time, without relying on indirect metrics such as the power factor, which are often unstable at high loads.
2. Construction of an internal median of the hourly power, used as a reference profile to identify deviations, losses, and atypical behavior. This allows objective detection of deficiencies compared to the typical behavior of the installation without the need for external reference data.
3. Comparison with climatically conditioned reference profiles, based on long-term climate models that take into account solar radiation, temperature, and other meteorological factors valid for the specific location of the installation. Through them, the real efficiency factor is calculated and cases of technical, not climatic, energy deficit are identified.
4. Analysis of the dynamic behavior of the inverter, including load, power changes over time (ramp rate), reactive intervention, and compliance with regulatory limits.

In addition, a spectral analysis of the quality of electricity is performed, including harmonic content and the presence of DC in the output.

The combination of these approaches leads to the construction of a unified, structured, and reproducible analysis framework that is applicable both for operational needs (including maintenance planning, production optimization, and early diagnostics) and for scientific evaluation of the efficiency of PV systems in different climatic and operating conditions.

Furthermore, the methodology is applicable not only at the individual inverter level but also in the context of analysis, where multiple sites are simultaneously compared on the same scale of efficiency and stability. This opens up opportunities for automated monitoring, site classification, predictive maintenance, and prioritization of interventions by operators and owners.

This study presents results based on data from a real 1 MW PV plant located in Southeastern Europe. The SCADA platform used provides a 5 min resolution, which allows for a reliable analysis of transients, dynamic loads, and power quality parameters. The constructed operating profile was used to assess a number of key indicators—including load, response to changing lighting, reactive interference, frequency stability, as well as overall system resilience under changing climatic and grid factors.

In conclusion, this study aims to offer an alternative to traditional KPIs by presenting a multi-layered, dynamic, and climate-normalized analysis based on real operational data and physically based calculations. The following sections of the article discuss the theoretical basis of the PV-inverter architecture, the rationale and objectives of the analysis, the methodology used for data processing and evaluation, the results of the application to the real system, as well as conclusions and recommendations for optimizing the operation of the inverters under real operating conditions.

2. Literature Review

The DC input operating profile of a grid-connected photovoltaic (PV) inverter is the result of interacting factors: conversion models and algorithms (DC/AC), MPPT algorithms and their response to dynamic changes in irradiance and temperature, filter, and control strategies, grid synchronization, as well as regulatory requirements for power quality and disturbance behavior. This review summarizes leading standards, key publications, and established methodologies for modeling and evaluating the operating profile, with a systematic focus on AC/DC efficiency, MPP tracking, harmonics, reactive power control, ramp-rate limitation, and performance assessment (PR/PI) metrics applicable to the conditions in Europe and the SEE region.

Inverters in distributed generation are subject to connection and interoperability requirements defined by IEEE 1547-2018 [1] and the European Network Code RfG (EU 2016/631) [2]. These regulate functions such as LVRT/HVRT, power factor control, and Volt/VAR/Volt/Watt modes, as well as requirements for detection and management of network anomalies. Limitations on harmonics and intermediate frequencies are covered by IEEE 519-2014 [3] and relevant IEC/EN standards (e.g., IEC 61000-3-12 for products >16 A to 75 A [4]). Reference is made to EN 50530:2010+A1:2013 [5] for the specific behavior of PV inverters during MPPT and overall efficiency testing. The monitoring and reporting of operational KPIs is standardized by IEC 61724-1:2021 [6] and IEC TS 61724-3:2016 [7]. The UL 1741 certification in North America (including the SA supplement for "advanced inverter" functions) specifies tests for network services and safety [8].

A generalized model of the converter and associated losses is critical to predicting the DC operating profile [9–16]. The Sandia Inverter Model [17] and its companion paper SAND2007-5036 (King, Gonzalez, Galbraith, Boyson) [15,16] provide a parametric description of the efficiency versus DC voltage, load, and "quasi-static" conditions. The model

allows the calculation of the expected AC power, DC requirements (including clipping and PS0 losses), and the corresponding DC current/voltage operating envelope in combination with array models (SAPM/PVWatts).

The Performance Ratio (PR) and Performance Index (PI) are widely used for operational evaluation. PR normalizes energy to reference radiation and installed power (IEC 61724-1) [6], while PI compares measured energy to model predicted energy and is less sensitive to seasonal temperature variations [18,19]. PR/PI in practice are analyzed together to detect degradation, system losses, or MPPT regression.

Comparative studies by Esram and Chapman [20] and later reviews [21–23] define a palette of MPPT methods—from classical P&O and IncCond to stochastic and intelligent (PSO/GA/ANN). In the context of the inverter "operation profile", the most important are the following:

1. The ability to quickly track rapid changes in irradiance (clouds, wind gusts);
2. Stability and low oscillation around the MPP in partial shading;
3. The interaction with DC bus limits and quasi-steady-state efficiency of the converter (avoiding frequent transitions to low-efficiency modes and clipping).

The standard EN 50530 [5] specifies tests for dynamic MPPT scenarios, allowing inter-inverter comparison.

The choice of LCL filter and current/voltage regulators determines the power quality, losses, and robustness to grid variations. The classic work by Liserre, Blaabjerg, and Hansen [9] provides a procedural design of an LCL filter and shows the trade-off between ripple attenuation and robustness. Advanced active damping approaches (Peña-Alzola et al.) [10] increase robustness to grid inductance variations and parallel inverters. The proportional-resonant (PR) controller in a steady-state $\alpha\beta$ frame [11] avoids the need for $d-q$ transformations and gives zero static error at 50 Hz, while also allowing selective harmonic compensation—key to meeting IEEE/IEC limits without excessive losses.

Synchronization is crucial for stability and accurate P/Q exchange. The structures SOGI-PLL/DSOGI-PLL [12–14] provide good filtering and fast adaptation to distortions and imbalances, maintaining stable inverter operation under disturbances. This directly affects the DC operating profile through dynamic loading of the DC bus and transient currents.

Investors and operators require limiting AC output fluctuations to reduce the impact on the grid. Studies by Marcos et al. [24,25] show that the minimum energy buffer required to meet a certain ramp-rate limit depends on the spectrum of irradiance fluctuations and the system configuration (fixed/tracking). This has a direct impact on the DC load profile of the inverter and on the choice of DC-link/battery.

Reliable radiation and temperature time series are the foundation for DC/AC profile modeling and normalized KPIs. PVGIS in Europe and its parent databases (Huld et al.) [26–29] are widely used, as is NASA POWER for global/regional applications [30,31]. ENTSO-E/C3S Pan-European Climate Database (PECD) for system adequacy analyses and climate scenarios provides homogenized solar generation time series valid for ERAA/planning [32–34]. The IEA PVPS Task 13 guidelines in operation [35–39] provide good practices for monitoring, O&M, and uncertainty assessment—useful for interpreting PR/PI and for diagnosing changes in the DC operating profile (fouling, degradation, thermal hotspots, PID, etc.).

Discussion and implications for design and operation:

1. Grid Compatibility: IEEE 1547/RfG requirements impose functions that change the current and reactive power setting and indirectly model the DC load. Enabled Volt/VAR/Volt/Watt control affects the MPP position under AC-side constraints.

2. Modeling and Verification: Sandia Inverter Model parameterization, validated against EN 50530, provides a robust relationship between DC conditions and AC output. PI is suitable for fleet comparisons and early regression detection.
3. Control and Filters: LCL + PR/active damping minimizes current harmonics and losses, improving efficiency over a wide range of load conditions, which is critical at low DC voltages/clouds.
4. Data and climate: Climate variability (fast cloudiness, dust episodes) for SEE (incl. Bulgaria) requires a valid hourly (or finer) resource from PVGIS/NASA POWER and, if necessary, climate normalization with PECD.
5. Ramp-rate limitation: Designing a minimum ramp-rate buffer according to [24,25] stabilizes the DC profile and reduces the number of transitions through inefficient operating points.

3. Description and Objectives of the Study

The modern PV inverter DC input operating profile is a product of standardized grid functions, dynamic MPPT algorithms, robust filter and PLL solutions, and quality climate data. The integration of these elements, according to the cited experience, increases production predictability, reduces degradation-induced PR/PI regressions, and facilitates grid compliance.

In this context, the present work proposes an integrated, physically informed approach for the analysis and evaluation of the operating profile of a DC/AC inverter in a real PV installation. The core of the approach is the recovery of the active AC power by the physical relationship $P_{AC} = P_{dc}\eta_{inv}$, which avoids numerical instabilities at $|\cos\varphi| \to 1$ and provides a reliable input for all subsequent metrics—percentile load levels (P_{95}, P_{99}, P_{max}), ramp-rate distribution, PF/PQ dissipation, and efficiency curve $\eta(P)$. An operational internal basis (hourly median power) is built above this layer, which serves as an early indication of "deficits compared to a typical day" without mixing with the contractual interpretation of curtailment. The profile is supplemented for official KPIs (PR and climate-consistent curtailment) with a climate reference $\hat{P}(t)$ obtained from PVGIS/PECD or NASA POWER regression.

The empirical basis is SCADA data with a 5 min resolution for the period of 25 January–15 April 2025 (local time), including DC-side measurements (string voltages/currents, P_{dc}), AC quality quantities (Q, $\cos\varphi$), and instantaneous inverter efficiency η_{inv}. The data are time-scaled, day/night filtered, and synchronized for reliable energy integrals, dynamic estimates, and checks against PQ-capability constraints. The climate time series are brought to the local time zone and interpolated to 5 min, with the capacity calibrated robustly (percentile scale/Huber) to achieve comparability between observation and potential.

The objectives of the study are threefold:

1. To build a detailed inverter operating profile—energy, load, dynamics, $\frac{PF}{PQ}$, and $\eta(P)$, on physically recovered active power;
2. To introduce an operational indicator for deficit relative to the internal median and to clearly distinguish it from curtailment;
3. To integrate a climate basis for reporting PR (daily and total) and climate-adjusted energy deficit $\sum(\hat{P} - P)_+$.

The contribution lies in the unification of physical recovery, robust time statistics, and climate matching into a reproducible analytical chain that is directly applicable to O&M diagnostics.

The structure of the described study aims for both technical rigor and operational utility, so that inverter profiling is transparent, comparable, and suitable for decision-making at the plant and grid operator levels.

4. Notations

The notations used in this study are given in Tables 1–9.

Table 1. Time, indices, and operators.

Symbol	Designation	Units	Range/Note
t	Time Moment (Time index)	—	Discretization 5 min (Median $\Delta t = 300$ s)
Δt	Time Step	s/h	$\Delta t = 300\ \text{s} = \frac{1}{12}\ \text{h}$
h	Hour of Day	h	$\text{h} \in \{0, \ldots, 23\}$
d	Calendar Date	—	Local Time (Europe)
$\sum t$	Sum of Times	—	For Energies/Units
$median\{\cdot\}$	Median	—	Sustainable Statistics
$Q_p\{\cdot\}$	p-percentile (quantile)	—	e.g., $Q_{0.95}$, 0.99
IQR	Interquartile Range	—	$Q_{0.75} - Q_{0.25}$
$(x)_+$	Positive Part	—	$\max(x, 0)$
(	\cdot	)	Absolute Value

Table 2. SCADA measurements (main channels).

Symbol	Designation	Units	Range/Note
$P_{dc}(t)$	DC Power to Inverter	kW	From Pdc(kW)
$\eta_{inv}(t)$	Inverter Efficiency	—	From $InvEfficient(\%)/100$
$P_{AC}(t)$	AC Active Power	kW	Restored: $P_{AC} = P_{dc}\eta_{inv}$
$Q_{ac}(t)$	Reactive Power	kVAr	From Qac(kVar)
$\cos\varphi(t)$	Power Factor (Sign)	—	From $\cos(\varphi)$
(	\mathrm{PF}	(t))	Absolute PF
$\overline{V}_{dc}(t)$	Aggregated DC Voltage	V	Average of Upv^* (V)
$\bar{I}_{dc}(t)$	Aggregated DC Currents	A	Average of Ipv^* (A)

Table 3. Derived quantities and energies.

Symbol	Designation	Units	Range/Note
E_{AC}	Total Produced Energy	kWh/MWh	$\sum_t P_{AC}(t)\Delta t$
$E_{AC,day}(d)$	Daily Energy	kWh	$\sum_{t \in d} P_{AC}(t)\Delta t$
$RR(t)$	Ramp Rate	kW/min	$\Delta P/\Delta t$ over 5 min
(	RR	_{95})	95th percentile of
P_{95}, P_{99}	Percentile P_{AC} Levels	kW	For “upper” levels
P_{max}	Observed P_{AC} Maximum	kW	No clipping if no plateau

Table 4. Internal (operational) bases and indicators.

Symbol	Designation	Units	Range/Note
$\hat{P}_{hour}(h)$	Internal Hourly Median Power	kW	"Typical Day" (Weather-Sensitive)
$\hat{E}_{hour}(t)$	Cumulative Energy on an Internal Basis	kWh	$\sum \hat{P}_{hour}\Delta t$
$PR^{*}_{daily}(d)$	Operational PR^{*} Relative to $\hat{P}_{hour}$	—	Median of $P/\hat{P}_{hour}$ per Day
$\mathcal{D}$	"Deficit" Intervals	—	Segments $P < 0.6\hat{P}_{hour} \geq 15$ min
ΔE_{hour}	Total Deficit Relative to $\hat{P}_{hour}$	kWh/MWh	$\sum_{t\in\mathcal{D}} \left(\hat{P}_{hour} - P\right)_{+}\Delta t$

Table 5. Climate references and models.

Symbol	Designation	Units	Range/Note
$\hat{P}(t)$	Climate Reference Power (Total)	kW	PVGIS/PECD/NASA model
$\hat{P}_{PVGIS}(t)$	Expected PV Power from PVGIS	kW	By geometry/losses
$\hat{P}_0(t)$	PVGIS Power Normalized (per 1 kW_p)	kW	For scale calibration
C	Scale to Real Capacity	kW/kW	$C \approx Q_{0.99}(P)/Q_{0.99}\left(\hat{P}\right)$
$CF(t)$	Capacity Factor (PECD)	—	0…1
$C_{\backslash *}$	Scale to $CF(t)$	kW	$\hat{P}_{PECD} = C_{\backslash *}CF$
$\hat{P}_{REG}(t)$	Regressive $\hat{P}$ (NASA)	kW	$aGHI + bT_2 + c\,WS + d$
$GHI(t)$	Global Radiation at Horizon	W/m^2 //Wh/m^2(h)	NASA POWER: hourly Wh/m^2
$T_2(t)$	Temperature at 2 m	°C	NASA POWER
$WS_{10}(t)$	Wind at 10 m	m/s	NASA POWER
C_{cert}	Nameplate/Certificate DC Peak Power	kWp	
ε_c	Relative Scale Error	—	$\frac{C - C_{cert}}{C_{cert}}$

Table 6. KPI against climate base.

Symbol	Designation	Units	Range/Note
$PR_{daily}(d)$	Daily PR	—	$\frac{\sum_{t\in d} P\Delta t}{\sum_{t\in d} \hat{P}\Delta t}$
$PR_{overall}$	Overall PR	—	$\frac{\sum_t P\Delta t}{\sum_t \hat{P}\Delta t}$
ΔE_{curt}	Climate-Friendly "Deficit" (Curtailment)	kWh/MWh	$\sum \left(\hat{P} - P\right)_{+}\Delta t$
$r(t)$	Residual against $\hat{P}$	kW	$r = P - \hat{P}$

Table 7. Geometry/design parameters.

Symbol	Designation	Units	Range/Note
$\boldsymbol{\theta_z(t)}$	Zenith Angle of the Sun	°	$\cos\theta_z$ in geometric base
$\boldsymbol{\gamma}$	Exponent in Geometric Base	—	$\hat{P} = C\cos^{\gamma}\theta_z$
$\boldsymbol{\beta}$	Inclination of the Modules	°	PVGIS parameter angle
$\boldsymbol{\psi}$	Azimuth (0° = South)	°	PVGIS parameter aspect
ILR	DC:AC Coefficient (Inverter Loading Ratio)	—	Design parameter

Table 8. Energy quality and limits.

Symbol	Designation	Units	Range/Note
$\boldsymbol{Q-P}$	Point in Plane PQ	kVAr − kW	$PF \approx 1 \Rightarrow Q \approx 0$
(	\mathrm{PF}	<0.95)	PF Deviation Indicator
TRIP/RESTART	Shutdown/Restart Events	—	Number and Times of Events

Table 9. Weights, calibration sets, and indicator function.

Symbol	Designation	Units	Range/Note
$\boldsymbol{\omega_t}$	Weight in Regression/Calibration	—	Larger on clear afternoons
$\boldsymbol{\mathcal{S}}$	Set of "Pure" Intervals	—	For C calibration
$\mathbf{1}\{\cdot\}$	Indicator Function	—	Optionally in algorithms

5. Theoretical Foundation

The architecture of the PV-inverter system includes a PV generator (panel array), modeled as a nonlinear current source; a DC/DC stage with MPPT (step-up/step-down) to a DC link with capacitance C_{dc}; and a three-phase DC/AC inverter with Space-Vector PWM, connected to the grid through an L or LCL filter and a synchronization system (PLL) and a cascade of regulators in dq coordinates.

The target values for monitoring/evaluation are the following:

- DC voltage V_{dc};
- DC current I_{dc};
- AC phase voltages/currents $v_{a,b,c}(t)$, $i_{a,b,c}(t)$;
- Active/reactive power P, Q;
- Power factor $\cos\varphi$;
- Inverter efficiency η;
- Internal temperature T_{int}.

The PV generator model is expressed by the current-voltage characteristic of the PV cell/string at illuminance G and temperature T:

$$I = I_{ph}(G,T) - I_0(T)\left[\exp\left(\frac{q(V-IR_s)}{nkT} - 1\right)\right] - \frac{V-IR_s}{R_{sh}}, \quad (1)$$

where

I_{ph}—photocurrent (proportional to G);
I_0—reverse saturation current;
R_s, R_{sh}—series/shunt resistance;
n—ideality;

q—electron charge;
k—Boltzmann's constant.
The power of the PV generator is

$$P_{pv}(V) = VI(V), \qquad \frac{dP_{pv}}{dV} = 0 \Rightarrow work\ in\ MPP \tag{2}$$

The energy balance and dynamics of the DC link are expressed by the average DC bus power:

$$P_{dc} = V_{dc} I_{dc} \tag{3}$$

and the charge of the capacitor guarantees a short-term buffer:

$$C_{dc} \frac{dV_{dc}}{dt} = i_{pv} - i_{inv} - i_{loss}, \tag{4}$$

where
i_{pv}—current from DC/DC to the bus;
i_{inv}—current to the inverter (averaged over one PWM period);
i_{loss}—losses (ESR, auxiliary loads).
The averaging model of the inverter and modulation is represented by averaging the PWM/Space-Vector PWM voltage at the output of an idealized full bridge (in phase):

$$v_x^* = m_x \frac{V_{dc}}{2}, \qquad x \in \{a, b, c\}, \tag{5}$$

where $m_x \in [-1, 1]$ is the modulation signal.
A vector form in $\alpha\beta$ is

$$\mathrm{v}_{\alpha\beta}^* = \frac{V_{dc}}{2} m_{\alpha\beta} \tag{6}$$

The filter and the grid connection are implemented using Clarke–Park transformations. The inverter is connected to the grid with phase voltages v_{abc} through an inductance L (or LCL). An L-filter with active losses R is used for simplicity.
Clarke transformation is

$$\begin{bmatrix} x_\alpha \\ x_\beta \end{bmatrix} = \frac{2}{3} \begin{bmatrix} 1 & -\frac{1}{2} & -\frac{1}{2} \\ 0 & \frac{\sqrt{3}}{2} & -\frac{\sqrt{3}}{2} \end{bmatrix} \begin{bmatrix} x_a \\ x_b \\ x_c \end{bmatrix} \tag{7}$$

Park transformation (synchronous frame with angle θ from PLL) is

$$\begin{bmatrix} x_d \\ x_q \end{bmatrix} = \begin{bmatrix} \cos\theta & \sin\theta \\ -\sin\theta & \cos\theta \end{bmatrix} \begin{bmatrix} x_\alpha \\ x_\beta \end{bmatrix} \tag{8}$$

The dynamics of currents in dq are

$$L \frac{di_d}{dt} = v_d^* - v_{g,d} - R_{i_d} + \omega L_{i_q}, \tag{9}$$

$$L \frac{di_q}{dt} = v_q^* - v_{g,q} - R_{i_q} - \omega L_{i_d}, \tag{10}$$

where
ω—grid corner frequency from the PLL;
$v_{g,d}$, $v_{g,q}$—mains voltage in dq.

The instantaneous powers in αβ are

$$p(t) = v_\alpha i_\alpha + v_\beta i_\beta, \tag{11}$$

$$q(t) = v_\alpha i_\beta - v_\beta i_\alpha \tag{12}$$

In a steady-state mode with synchronized dq (PLL aligns v_g along the d-axis, $v_{g,q} \approx 0$),

$$P = \frac{3}{2} v_{g,d} i_d, \qquad Q = \frac{3}{2} v_{g,d} i_q \tag{13}$$

The power factor is

$$PF = \sin\varphi = \frac{P}{\sqrt{P^2 + Q^2}} \tag{14}$$

The energy for an interval Δt is

$$E = \int_{t_0}^{t_0+\Delta t} P(t)dt \approx \sum_k P_k \Delta t_k \tag{15}$$

Closed-loop control is defined by a typical cascade including

- PLL: estimates $\hat{\theta}$, $\hat{\omega}$ from v_{abc} through a PI controller on $v_q \to 0$.

Outer loop—one of two strategies:

- Maintaining V_{dc} (or output active power P^*);
- MPPT of DC/DC, which sets a reference power/current to the inverter.

Inner current loop in dq:

$$i_d^* = \frac{2}{3}\frac{P^*}{v_{g,d}}, \qquad i_q^* = \frac{2}{3}\frac{Q^*}{v_{g,d}}, \tag{16}$$

PI controllers with decoupling terms $\pm\omega L_{i_{q,d}}$ generated v_d^*, v_q^*, which are converted into modulations $m_{a,b,c}$ by SVM.

The total losses are

$$P_{loss} = P_{cond} + P_{sw} + P_{filt} + P_{aux} \tag{17}$$

The efficiency of the inverter is

$$\eta_{inv} = \frac{P_{AC}}{P_{DC}} = \frac{P}{V_{dc} I_{dc}} \tag{18}$$

The simplified thermal RC-grid model is

$$C_{th}\frac{dT_j}{dt} = P_{loss} - \frac{T_j - T_a}{R_{th,ja}}, \tag{19}$$

where

T_j—crystal temperature;
T_a—ambient temperature;
$R_{th,ja}$—total thermal resistance.

The limitations and permissible operating range are

- Current limitation:

$$\sqrt{i_d^2 + i_q^2} \le I_{\max} \tag{20}$$

- Voltage/modulation limitation:

$$\left|\mathrm{m}_{\alpha\beta}\right| \leq m_{\max} \tag{21}$$

- PQ capabilities:

$$\left(\frac{P}{S_{\text{rated}}}\right)^2 + \left(\frac{Q}{Q_{\max}}\right)^2 \leq 1 \tag{22}$$

- Harmonic norms:

$$\mathrm{THD}_I = \frac{\sqrt{\sum_{n=2}^{\infty} I_n^2}}{I_1} 100\% \tag{23}$$

The operating profile is defined as the time trajectory of the operating points:

$$X(t) = [V_{dc}(t), I_{dc}(t), P(t), Q(t), PF(t), T_{int}(t), \ldots], \tag{24}$$

collected with a step Δt. This profile is used for the following:

- Energy balances $\int Pdt$;
- Efficiency assessment/MPPT use;
- Verification of compliance with restrictions (current, PF, THD);
- Correlations with external factors (illuminance, temperature, market regimes).

This theoretical framework sets the mathematical basis for subsequent methods for profile analysis and evaluation (identification, optimization, statistical testing), as well as for calculating the key indicators η, P, Q, PF, THD, T_j.

Explicit temperature/illuminance corrections and an MPPT criterion for the PV source are used to estimate expected MPP points for real changes in G, T, such as the following:

- The photo part is

$$I_{ph}(G,T) \approx \frac{G}{G_{ref}}\left[I_{sc,ref} + \alpha_I\left(T - T_{ref}\right)\right] \tag{25}$$

- The open voltage is

$$V_{oc}(G,T) \approx V_{oc,ref} + \beta_V\left(T - T_{ref}\right) + nV_T \ln\frac{G}{G_{ref}}, \qquad V_T = \frac{kT}{q} \tag{26}$$

- MPPT "incremental conductivity" (algorithmic criterion) is

$$\left.\frac{dI}{dV}\right|_{MPP} = -\frac{I}{V} \tag{27}$$

The quantitative estimates of the filtering and the required C_{dc} for the DC/DC stage are implemented through static connections and ripples, such that the following arises:

The ideal converters (on average) are

$$\text{Buck}: V_{dc} = DV_{pv}, \qquad \text{Boost}: V_{dc} = \frac{V_{pv}}{1-D}, \qquad \text{Buck} - \text{Boost}: V_{dc} = \frac{D}{1-D}V_{pv} \tag{28}$$

The pulsations from the commutation are

$$\Delta I_L \approx \frac{V_L D}{L f_{sw}}, \qquad \Delta V_C \approx \frac{\Delta I_L}{8 C f_{sw}} \tag{29}$$

The double-frequency ripple of a DC link (from power exchange with the grid) is

$$\Delta V_{dc} \approx \frac{P_{2\omega}}{2\omega C_{dc} V_{dc}} \tag{30}$$

Modulation is the relationship "module index → fundamental RMS" and is

$$V_{1,rms} = k_{\text{mod}} m V_{dc},\ m = \max|m_x|, \tag{31}$$

and allows for directly predicting the output voltage at a given m (k_{mod} depends on SPWM/SVPWM).

The expanded definition of PF with a distortion factor, i.e., PF decomposed into "displacement" and "distortion" parts, is

$$PF = \frac{P}{\sqrt{P^2 + Q^2}} = \underbrace{\cos\varphi_1}_{1st\ harmonic\ shift} \underbrace{\frac{1}{\sqrt{1 + THD_I^2}}}_{harmonics\ influence} \tag{32}$$

The metrics for the profile section in the discrete case are the following efficiencies:

$$E_{AC} = \sum_k P_k \Delta t, \qquad E_{DC} = \sum_k V_{dc,k} I_{dc,k} \Delta t \tag{33}$$

$$\eta_{inv} = \frac{P_k}{V_{dc,k} I_{dc,k}}, \qquad \eta_{MPPT} = \frac{\sum_k P_k}{\sum_k P_{MPP,k}}, \qquad \eta_{tot} = \frac{E_{AC}}{\sum_k E_{DC}} \tag{34}$$

The measurable harmonic power quality indicators are as follows:

- THD (from FFT/DFT):

$$THD_I = \frac{\sqrt{\sum_{n=2}^{\infty} I_n^2}}{I_1}, \qquad THD_V = \frac{\sqrt{\sum_{n=2}^{\infty} V_n^2}}{V_1} \tag{35}$$

- TDD and DC component:

$$TDD = \frac{\sqrt{\sum_{n=2}^{\infty} I_n^2}}{I_{rated}}, \qquad I_{dc} = \frac{1}{T}\int_0^t i(t)dt \tag{36}$$

A discrete-time DFT/FFT in the practical implementation is used on a 10-period window (50 Hz; 200 ms) synchronized to the mains frequency, respectively, 12 periods at 60 Hz, which provides $N = f_s T \approx 12{,}800$ Hz·0.2 s = 2560 samples and $\Delta f = \frac{f_s}{N} = 5$ Hz, as required by IEC 61000-4-7 (Class A, grouping/subgrouping). A rectangular window over an integer number of periods is used (minimizing leakage), the determination of the fundamental is achieved by DFT at $k \approx 50$ Hz with frequency tracking, and I_{DC} is estimated as a time average value in the window. THD_I, THD_V, and TDD are calculated according to (35) and (36) on the 2nd to 50th harmonic.

The practical implementation of the $THD/TDD/I_{DC}$ estimators uses FFT over 10–12 period windows, as is standard in PQ estimation; the numerical uncertainty and the influence of noise/quantization are summarized in Section 7.

The automated check is carried out using PQ capabilities and constraints through explicit formulas:

- "Ellipse" of the work area:

$$\left(\frac{P}{S_{rated}}\right)^2 + \left(\frac{Q}{Q_{\max}}\right)^2 \leq 1, \qquad Q_{\max}(P) = \sqrt{S_{rated}^2 - P^2} \tag{37}$$

- Limit on required minimum PF:

$$|Q| \leq |P| \mathrm{tg}(\arccos PF_{\min}) \tag{38}$$

The time-series indicators (statistics and dynamics) are key to assessing a "profile-in-time", such as the following:

- Means and variance:

$$\overline{P} = \frac{1}{N}\sum_k P_k, \qquad \sigma_P^2 = \frac{1}{N-1}\sum_k \left(P_k - \overline{P}\right)^2 \tag{39}$$

- Ramp rate (rate of change):

$$RR_k = \frac{P_k - P_{k-1}}{\Delta t}, \qquad RR_k^{\%} = \left(\frac{P_k - P_{k-1}}{S_{rated}}\right)\frac{100}{\Delta t} \tag{40}$$

- Capacity factor (CF) and performance ratio (PR):

$$CF = \frac{E_{AC}}{S_{rated} T_{period}}, \qquad PR = \frac{E_{AC}}{G_{POA} A \eta_{ref}} \tag{41}$$

The normative metrics are used to provide a quantitative assessment of time outside the permissible limits:

$$\Delta V\% = 100\frac{|V_1 - V_{nom}|}{V_{nom}}, \qquad \Delta f = f - f_{nom}, \qquad t_{out} = \sum_{k:infraction} \Delta t, \qquad r_{out} = 100\frac{t_{out}}{T_{period}} \tag{42}$$

6. Methods and Algorithms for Analysis and Evaluation

The used methods for analysis and evaluation are described sequentially as follows.

First, data preparation is performed: the individual channels (DC voltage and current, AC voltages and currents, phase/φ, possibly illuminance and temperature) are translated to the same time grid, for example, every Δt minutes. If there is haven latency between the channels, it is compensated by aligning with maximum cross-correlation, so that short-term changes in V_{dc} and P coincided. Small gaps are interpolated (linearly or with a spline), and longer ones are marked and excluded from the integral estimates. Noisy measurements and spikes are smoothed with a moving median or Savitzky–Golay filter; if waveforms $v(t)$, $i(t)$ are available, the Kalman filter gives clean estimates for the fundamental components and the phase. Next comes the natural "day/night" mask by the V_{dc} threshold or illumination, to avoid contaminating efficiency and MPPT metrics with night points.

The primary features are extracted from each time point once the data is cleaned: instantaneous active and reactive power P and Q (from the fundamental V_1, I_1, φ), power factor PF, inverter efficiency η_{inv}, and rate of change RR. The harmonics I_n, V_n and from them THD_I, THD_V, and TDD are given where there are sufficient samples of waveforms, via spectral analysis using FFT. All powers are normalized in per-unit relative to S_{rated}, so that they can be compared across days, seasons, and different objects on the same scale.

The time analysis is performed at several levels. The average, variations, and empirical distribution of the ramp rate are estimated in moving windows (hour, day), which shows how well the inverter "follows" the dynamics of the input and the grid without excessive

excitability. The detection of changes (e.g., CUSUM or PELT) captures structural transitions: clouds, clipping when reaching DC/AC limits, curtailment on operator command or restart. Clusterization (e.g., *k*-means or DBSCAN) is applied on vectors $[p, q, PF, \eta, RR, THD]$ to recognize typical operating modes: in this way, "normal operation", "reactive maintenance", "limit operation", "grid limitation", "switching off/on", etc., are separated.

The frequency view is complementary: in short windows of 10–12 network periods, the FFT gives the amplitudes of the low odd harmonics (5th, 7th...), the total THD, and the DC component. These are compared with the permissible limits; "time outside the norm" and a relative share are accumulated, which later became one of the key KPIs for power quality.

The actual quantitative assessment also requires model identification. An efficiency map $\eta = f(P, T)$ is constructed from the data (P, T), which is usually a smooth polynomial or spline surface, estimated with robust methods (Huber, RANSAC), and the reliability is checked with cross-validation and bootstrap confidence intervals. Separately, a simple loss model P_{loss} is calibrated as a function of current and switching, e.g., $k_0 + k_1 I + k_2 I_2 + k_3 f_{sw} V I$, by nonlinear least squares (Levenberg–Marquardt). There are enough points (V_{dc}, I_{dc}) along the "envelope" during the day, which allowed for calibration and construction of the single-diode PV model. This is allowed for estimating $P_{MPP}(G, T)$ and hence MPPT efficiency η_{MPPT}. The parameters are tracked online (RLS/EKF) for long time series to capture degradation or changes in settings. The algorithm for THD/TDD and DC component estimation is as follows:

Data source: Class-A PQ analyzer (see Section 7) with $f_s = 12.8$ kHz, 16-bit ADC, and analog anti-aliasing at the input.

Window and spectral processing: DFT/FFT over 10 consecutive periods (50 Hz; 200 ms), rectangular window, $N = 2560$, $\Delta f = 5$ Hz; grouping/subgrouping according to IEC 61000-4-7 up to the 50th harmonic; the fundamental is determined by tracking the network frequency (IEC 61000-4-30).

Anti-aliasing and frequency range: the analysis is limited to 2.5 kHz (50th harmonic), at $f_{Nyquist} = 6.4$ kHz, which, together with the analyzer's analog anti-alias filter, eliminates aliasing artifacts.

Metrics:

- THD_I, THD_V by (35); TDD normalized to the nominal current of the PF/PSC; I_{DC} as time-averaged value in the window.
- Aggregation to 5 min scale: median and 95th percentile of all 200 ms estimates in the interval; synchronization with SCADA by timestamp (NTP, 5 min grid).

Reliability and uncertainty: $THD/TDD/DC$ uncertainty includes contributions from quantization (16-bit), noise/SNR, limited window length, and network frequency variations; estimated as σ_{THD} and 95% CI by bootstrapping over days/intervals (see Section 7). Comparison to IEEE 519 and IEC 61000-3-12 is reported with the indicator "time fraction outside the norm".

Note: SCADA at 5 min does not contain waveforms; the harmonic channel is separated from the PQ analyzer (see Section 7).

6.1. Modeling and Parameterization of the Efficiency $\eta(P, T)$

To model the relationship between the efficiency of the inverter and its operating parameters, such as active power and temperature, a two-dimensional continuous and smooth model of the third-degree tensor B-spline type is used, defined on normalized dimensionless variables $p = \frac{P_{AC}}{S_{rated}}$ and $\tau = \frac{(T - 25\ ^\circ\mathrm{C})}{10}$.

This choice provides sufficient flexibility to describe nonlinear dependencies under different loads and temperature regimes without leading to overfitting or instability of the estimates.

The functional form of the model is given as

$$\eta(p,\tau) = \beta_0 + \sum_i \beta_i B_i^{(3)}(p) + \sum_j \gamma_j C_j^{(3)}(\tau) + \sum_i \sum_j \delta_{ij} B_i^{(3)}(p) C_j^{(3)}(\tau), \tag{43}$$

where $B_i^{(3)}(p)$ and $C_j^{(3)}(\tau)$ are cubic spline basis functions for load and temperature, and β_i, γ_j, δ_{ij} are the corresponding model parameters. The nodes of the spline are located on quantiles of the available data, which allows for a denser representation in frequently observed regions (around the nominal load and typical temperatures).

The fitting of the surface $\eta(P,T)$ is performed by robust regression with Huber loss, combined with a RANSAC procedure to exclude outliers caused by atypical modes, restarts, or unstable measurements. This approach reduces the influence of isolated errors and ensures the robustness of the estimates even with noisy SCADA data.

To ensure physical plausibility of the dependence, monotonicity and range constraints are imposed, with the efficiency η being limited to the interval $[0,1]$, by applying weak regularization that penalizes negative slopes $\frac{\partial \eta}{\partial p} < 0$ at low loads and excessively large temperature effects $\frac{\partial \eta}{\partial \tau} > 0$.

The model is identified using the Huber function minimization method with regularization terms ensuring smoothness of the surface along both axes (so-called P-splines). This ensures a smooth change in efficiency over load and temperature, without artificial interruptions.

The resulting parameterization describes the real efficiency surface $\eta(P,T)$ with high stability and is the basis for calculating confidence intervals and validation metrics (MAE, RMSE).

The efficiency model fitting procedure $\eta(P,T)$ is based on a sequential algorithm that combines data preprocessing, robust fitting, and metrologically meaningful parameterization. The first step involves selecting a reliable training set consisting only of daily intervals with normal inverter operation (without TRIP/RESTART events, reactive power limitations, or clear anomalies). The data are pre-filtered by the illuminance criterion (UDC > 100 V) and by the confidence interval of the measured efficiency ($0.85 < \eta < 1.0$), using the 5 min SCADA resolution.

The measured values of active power after filtering and temperature are normalized by the transformations $p = \frac{P_{AC}}{S_{rated}}$ and $\tau = \frac{(T - 25\ ^\circ\mathrm{C})}{10}$, which ensures large-scale comparability and numerical stability of the calculations. Based on these normalized coordinates, a network of B-spline bases is constructed, typically with six nodes along the load axis and five nodes along the temperature. The resulting basis system gives a flexible but smooth surface approximation.

The actual fitting is performed by robust regression with Huber loss, with the objective function to minimize being

$$J(\theta) = \sum_k w_k \rho_\delta(\eta_k - \eta(p_k, \tau_k; \theta)) + \lambda_P \int (\eta_{pp})^2 dp + \lambda_T \int (\eta_{\tau\tau})^2 d\tau + \int\int (\eta_{p\tau})^2 dp d\tau \tag{44}$$

where ρ_δ is the Huber function, λ_P, λ_T, λ_{PT} are regularization coefficients, and w_k are weights inversely proportional to the metrological uncertainty of the corresponding observations. The weights are calculated based on the accuracy classes and standard deviations σ_V, σ_I, σ_η, presented in Section 7, to account for larger uncertainty at lower loads.

Outliers caused by transients or disturbances are eliminated in advance by a RANSAC procedure with a threshold determined by the median deviation of the residuals (MAD).

The remaining model parameters are estimated by an iterative Levenberg–Marquardt algorithm, with initial values determined by a linear approximation of the $\eta(P)$ dependence at a nominal temperature.

Range constraints ($0 \leq \eta \leq 1$) after each iteration and monotonicity with respect to the load are applied to ensure physical consistency, penalizing negative derivatives $\frac{\partial \eta}{\partial p} < 0$. The process continues until a stable minimum of the function $J(\theta)$ is reached with a relative change below 10^{-4} between successive iterations.

The final result is a parameterized set of coefficients $\{\beta_i, \gamma_j, \delta_{ij}\}$, through which the surface $\eta(P, T)$ can be calculated for any combination of load and temperature. The resulting model provides high smoothness and robustness to extrapolation beyond the most frequently observed regimes, while preserving the physical interpretation of the efficiency and allowing subsequent calculation of confidence intervals and validation metrics (MAE, RMSE).

6.2. Model Validation

The validation of the efficiency model $\eta(P, T)$ aims to verify how well the parameterized surface reproduces the actually observed efficiency values under different load and temperature regimes. Leave One Day Out (LODO-CV) and 10-fold blocked cross-validation (10-fold CV) are applied for this purpose, in which the data are divided into non-overlapping daily blocks so as to avoid temporal correlation between the training and test sets.

The model is re-estimated on all days except one, and errors are calculated on the excluded day at each iteration. The accuracy of the model is assessed using two standard metrics:

$$MAE = \frac{1}{N}\sum_{k=1}^{N}|\eta_k - \hat{\eta}_k|,\ RMSE = \sqrt{\frac{1}{N}\sum_{k=1}^{N}(\eta_k - \hat{\eta}_k)^2}, \tag{45}$$

where η_k are the measured efficiency values and $\hat{\eta}_k$ are the model predicted ones. Calculations are performed in both absolute units (0–1) and percentage points (p.p.) to ensure comparability with metrological specifications.

In addition to the mean errors, the distributions of the residuals $(\eta_k - \hat{\eta}_k)$ over load and temperature are also analyzed. No systematic deviations are observed, while the mean value of the residuals is close to zero, and the variance remains almost constant over the entire operating range. This confirms that the model is not biased towards certain load or temperature ranges.

A bootstrap procedure by days (B = 1000 resampling) is used to estimate the confidence intervals. The model is recalculated for each resampled set, and the 2.5th and 97.5th percentiles of the predictions are derived for each grid point (P, T), which form a 95% confidence interval. The resulting bands are narrow in the nominal region ($0.7 < \frac{P}{S_{rated}} < 1.0$) and widen towards low loads, where a greater influence of noise and temperature is observed.

6.3. Confidence Intervals and Graphical Representation

Confidence intervals (CIs) are calculated based on a bootstrap procedure by days to provide a quantitative assessment of the reliability of the performance model $\eta(P, T)$. This approach reflects the real variability of the data resulting from meteorological conditions, load dynamics, and metrological uncertainty of the channels in the SCADA system.

The procedure involves 1000 bootstrap iterations, where the daily observation intervals are selected with repetition, and for each sample, the model $\eta(P, T)$ is recalculated entirely with Huber regression and P-spline regularization. A set of predicted values $\eta^{(b)}(p, \tau)$ is obtained for each point of the grid (p, τ), from which the 2.5th and 97.5th percentiles are

derived as the boundaries of a 95% confidence interval. This ensures that in 95% of the cases, the true efficiency of the inverter falls within this range.

The results show that the confidence intervals are narrowest in the nominal load region ($0.7 < \frac{P}{S_{rated}} < 1.0$) and at moderate temperatures (20–35 °C), where the volume of data is largest and the noise in the measurements is minimal. The intervals widen at low powers ($\frac{P}{S_{rated}} < 0.3$) or at extreme temperatures (below 10 °C and above 50 °C), reflecting the higher uncertainty and stronger nonlinearity of the $\eta(P, T)$ relationship.

The validated efficiency model and the resulting $\eta(P, T)$ surface are further illustrated and discussed in Section 7.2, where the numerical results and figures are presented.

The developed efficiency model $\eta(P, T)$ provides a reliable and physically justified relationship between the inverter load, the ambient temperature, and its real conversion efficiency. A smooth and stable description of the efficiency surface is achieved by applying a two-dimensional B-spline approximation and robust estimation methods (Huber and RANSAC), which preserves the correct behavior of the system over the entire operating range. Validation by blocked cross-validation and bootstrap estimation of confidence intervals confirms the high accuracy of the model and its robustness to noise and random deviations in measurements.

The resulting parameterization allows for predicting the efficiency at different combinations of temperature and load, thus providing an analytical basis for assessing energy losses, temperature sensitivity, and seasonal variations in the inverter operation. In addition, the model can be used for early detection of degradation, analysis of operational trends, and creation of digital twins of inverter systems. Its inclusion in the analysis methodology increases the diagnostic capabilities of SCADA monitoring and supports the optimization of operating modes, which leads to more precise management and prediction of the energy efficiency of the photovoltaic installation.

6.4. Capacity Calibration and Sensitivity of $\frac{PR}{\Delta E}$

Here, we use PVGIS "per-1 kWp" power $P_0(t)$ and scale it by C to obtain the climate reference $\hat{P}(t) = C\hat{P}_0(t)$ (Table 5). In addition to the percentile scaling $C_Q = \frac{Q_{0.99}\{P\}}{Q_{0.99}\{\hat{P}_0\}}$, the capacity is validated against the nameplate/certificate DC peak C_{cert} (kWp). When available, PVGIS is queried with $peakpower = C_{cert}$ to produce $\hat{P}^{(cert)}_{PVGIS}(t)$. If a small residual bias exists on clear-noon windows, a multiplicative correction is applied $g = \frac{Q_{0.99}\{P\}}{Q_{0.99}\{\hat{P}^{(cert)}_{PVGIS}\}}$.

The impact of a capacity-scale error $\varepsilon_C = \frac{C - C_{cert}}{C_{cert}}$ on KPIs is closed-form:

$$PR(C) = \frac{\sum_t P\Delta t}{C\sum_t C\hat{P}_0\Delta t} \Rightarrow \frac{PR(C)}{PR(C_{cert})} = \frac{1}{1+\varepsilon_C} \approx 1 - \varepsilon_C, \tag{46}$$

i.e., a +2% scale overestimates biases PR by $\approx -2\%$ (relative). For the climate-aligned shortfall,

$$\Delta E(C) = \sum_t \left(\hat{P}(t) - P(t)\right)_+ \Delta t \tag{47}$$

$$\frac{\partial \Delta E}{\partial C} = \sum_{t:\hat{P}(t)>P(t)} \hat{P}_0(t)\Delta t \Rightarrow \Delta E(C+\delta C) \approx \Delta E(C) + \delta C \sum_{t:\hat{P}>P} \hat{P}_0(t)\Delta t, \tag{48}$$

with the bound $|\Delta E - \text{bias}| \leq |\delta C| \sum_t \hat{P}_0(t)\Delta t$. Here, is report the observed ε_C and a small scenario table for $C\cdot(1 \pm 1\%, 1 \pm 2\%)$.

The practical capacity verification is performed in three steps: (i) a request to PVGIS with $peakpower = C_{cert}$ to generate $\hat{P}PVGIS(cert)(t)$; (ii) percentile control on the "clean" noon windows through the multiplier $g = Q_{0.99}\{P\}/Q_{0.99}\{\hat{P}PVGIS(cert)\}$; (iii) reporting

$\varepsilon_C = \frac{C - C_{cert}}{C_{cert}}$ and recalculating PR and ΔE for $\{C, C_{cert}\}$. The relative systematic error at $\delta_C = \frac{C}{C_{cert}-1}$ in PR is exactly (46), and the one-sided effect on ΔE is given by (48).

The climate potential only in the hours in which $\hat{P} > P$ is

$$\dot{E}_{>} = \sum_{t:\hat{P}>P} \hat{P}(t)\Delta t = C_{cert} \sum_{t:\hat{P}>P} \hat{P}_0(t)\Delta t \tag{49}$$

and gives the one-sided (in sign) upper bound by (48):

$$|\Delta E(C(1+\varepsilon_C)) - \Delta E(C)| \leq \varepsilon_C \dot{E}_{>} \tag{50}$$

If $\varepsilon_C > 0 \Rightarrow \Delta E$, this can increase at most by $\varepsilon_C \dot{E}_{>}$. If $\varepsilon_C < 0 \Rightarrow \Delta E$, this decreases modulo by $\leq |\varepsilon_C| \dot{E}_{>}$.

The normalized form of $\Delta E(C)$ is

$$\frac{\Delta E(C(1+\varepsilon_C)) - \Delta E(C)}{\Delta E(C)} \lesssim |\varepsilon_C| S_{\Delta E},\ S_{\Delta E} := \frac{\dot{E}_{>}}{\Delta E(C)} \tag{51}$$

Table 10 shows that at ±1–2% scale error PR scales exactly by $\frac{1}{1+\varepsilon_C}$, while the influence on ΔE is one-sided and limited only to the hours with $\hat{P} > P$, as follows from (46)–(48).

Table 10. Scenario check for capacity scaling $C \cdot (1 \pm 1\%, 1 \pm 2\%)$.

Scenario $C \to C(1+\varepsilon_C)$	ε_C (Relative)	PR Multiplier = $\frac{1}{1+\varepsilon_C}$	One-Sided Upper Bound for ΔE (Absolute)
−2%	−0.020	1.0204	$\leq 0.02\dot{E}_{>}$
−1%	−0.010	1.0101	$\leq 0.01\dot{E}_{>}$
+1%	+0.010	0.9901	$\leq 0.01\dot{E}_{>}$
+2%	+0.020	0.9804	$\leq 0.02\dot{E}_{>}$

ε_C is the relative change in capacitance; $\dot{E}_{>}$ is the climate potential only in the hours in which $\hat{P} > P$.

The evaluation in the PQ-plane is geometrically straightforward: the density of points is visualized, and we check what proportion of the time remains inside the permissible region (the ellipse of possibilities) and above the minimum required power factor. If the inverter follows a static $Q(V)$ characteristic (droop), the regression $Q = f(V)$ and the errors against the given curve indicate the quality of the reactive service.

Rules and machine learning are combined for events and anomalies. Clipping is recognized by a plateau of p close to 1 at a high G and stable V_{dc} by a persistent shift $P \ll P_{MPP}$ under normal DC conditions and/or active Q or PF commands; tripping—by a sharp drop in P and V_{dc}. Algorithms such as Isolation Forest or LOF are marked rare, multidimensional deviations. The duration and energy effect ΔE for each event are calculated against an appropriate counterfactual basis (e.g., P_{MPP} or the expected $\hat{P}$ from a model).

Forecasting also helped the evaluation: short-term ARIMA/SARIMAX models (with illumination and temperature as exogenous variables) or nonlinear methods such as gradient boosting and neural networks are given an "expected profile." Large systematic residuals (RMSE, MAE, Theil's U) are signaled degradation, contamination, or incorrect settings.

Finally, each KPI comes with a reliability measure. Bootstrapping by days gave 95% intervals for η, η_{MPPT}, PR, etc., and the standard error distribution (e.g., $Var(P) \approx I^2\sigma_V^2 + V^2\sigma_I^2$) translates the sensor accuracy classes into performance uncertainties. The results are presented in easy-to-read diagrams: density maps in PQ, heat maps of $\eta(P, T)$, timelines with marked events, histograms of ramp rate, and spectral "combs" of harmonics.

Thus, the entire path, from data cleaning to regulatory compliance and diagnosis, remains transparent and reproducible, and the inverter's operating profile is evaluated not only numerically but also contextually in relation to the plant mode and grid conditions.

The inverter is started by searching for the maximum power of the PV array. The simplest and most widely accepted approach is "Perturb and Observe": the controller slightly changes the set voltage or current of the array, and we watch how the output power changes. If the change is in the "right" direction, it continues; if not, it takes the reversed course. The step is made adaptive in order not to oscillate unnecessarily around the maximum, i.e., larger when it is far from the MPP (to quickly catch up), and small when it is already close (for low oscillation losses). A more precise option, known as "incremental conductance", not only looks at the direction of change but also compares the slope of the IV curve at the moment with that at the maximum. There, the slope satisfies a simple relationship between current and voltage; if the measurements show that this is to the left of this point, the controller increases the voltage, if this is to the right—it decreases it. The intelligent variants such as fuzzy logic and small neural networks perform even better when conditions are changed abruptly (clouds, strong wind): they connect the "error" and "rate of change" with smooth control actions and they can "guess" the good reference directly from illumination and temperature. The so-called "extreme search" is used in applications where one does not want to rely on models: a low-amplitude sine wave is superimposed on the reference, and from the power response, through demodulation and filtration, the direction towards the maximum is extracted without losing stability.

The inverter must "lock" the phase and frequency to properly match the grid. This is achieved by a PLL (phase-locked loop) in a synchronous frame: the measured three-phase voltage is rotated in dq coordinates, with the regulator forcing the "quadrature" component to zero, i.e., a sign that the rotation is synchronized with the grid. Narrowband (notch) filters or double synchronous frames are added for distorted or unbalanced voltages to suppress parasitic components around twice the grid frequency and to avoid "swinging" of the estimated phase.

Above the synchronization is the "outer" loop, the one that determines how much active and reactive power the inverter should deliver. It maintains in one mode a constant DC voltage on the bus and it converts the deviation from the set value into a target active power. The MPPT module dictates in the other mode (more typical for PV) the desired active power, and dispatcher requirements or agreed settings determine the reactive power. Reference currents are formed from these two targets in the dq synchronous frame: the active component flows along the d–axis, and the reactive component flows along the q–axis. The active power command is passed through a ramp-rate limiter that prevents sudden jumps in order to avoid unnecessary stress on the equipment and the grid.

The "inner" current loop is the fastest and keeps the real currents tightly around their references. The mathematics in the dq framework show cross-connections between the axes, so decoupling terms are added to the control laws, which "reset" them, and the main problem is left to ordinary PI regulators. Predictive options are used when even faster dynamics are pursued or switching is reduced: it is calculated with a discrete model from one sample ahead what voltage needs to be applied now to place the current exactly where it is needed in the next clock cycle. This is a "deadbeat" idea, and in a more general form—model-predictive control, in which the error and the number of switching are minimized.

The voltage commands are sent to the power section via PWM. Comparison with a triangular carrier in classical sine wave modulation gives good results, and adding a third harmonic extends the linear range. Vector modulation (SVPWM) uses the geometry of the six power vectors of the inverter and distributes the time of the active and zero states so as

to recreate the desired "voltage" vector with a minimum number of switches and about a 15% higher effective range.

There is a filter between the inverter and the grid, often of the LCL type, which smooths out high-frequency harmonics. However, it carries its own resonance. Active damping (which heat up) is more elegant instead of putting in large passive dampers: The current or voltage of the filter capacitor is measured and fed back with a small coefficient to the control signal, which "killed" the resonance without additional losses.

The quality of the current to the grid is often adjusted with regulators sensitive to sinusoidal references, the so-called PR controllers. They are operated in the stationary frame and they have a resonance exactly at the grid frequency (and optionally—at the 5th, 7th, etc., harmonics), so that they maintain zero static error for pure sinusoids and suppress specific harmonic pollution.

All of these loops rely on measurements, and they come with noise and gaps. This is where estimators come in: a discrete Kalman filter extracts fundamental amplitudes and phase from noisy waveforms, and recursive least squares or extended Kalman are used as "online" estimate parameters—inductances, DC link capacitances, even PV model parameters. This allows the control to adapt to aging, temperature drifts, and real-world changes in the system.

Forecasts and event detection on the analytical side complement operational management. Classic seasonal ARIMA models with exogenous variables (illuminance, temperature) provide an expected active power profile for the next hours, while more flexible methods such as gradient boosting and small neural networks capture nonlinearities and interactions. The difference between the actual and expected behavior (residuals) is monitored; accumulated systematic offset suggests panel contamination or non-ideal settings. Events are captured both with simple rules (clipping when limit is reached, curtailment on operator command, shutdown/restart) and with statistical tests for change and "anomaly analysis" (Isolation Forest, LOF), which signal rare and potentially critical deviations.

The P and Q commands are "designed" in the permissible range since the inverter is operated under regulatory and hardware constraints—the nominal apartment power, minimum power factor, ramping limits. This is a small real-time optimization problem that ensures that the following reference currents are feasible and compliant with the norms. Above all, there is thermal protection: a simple but reliable RC modeling of the temperature of the power elements is allowed to smoothly reduce the active power when the temperature approaches a critical one, and to restore it with hysteresis to avoid "chattering".

In practice, the settings are made hierarchically: the fastest is the current loop, above it is the PLL, and the slowest is the external power or DC voltage loop. The filters on the measurements are selected to attenuate noise above the operating frequencies of the loops, without introducing delays that would destabilize them. The inverter extracts the maximum possible energy from the PV array when all these "layers" work in concert, maintains a stable and quality injection into the grid, and reacts predictably to changes and anomalies. This is what is called a well-evaluated and well-managed "operating profile".

The hourly internal median $P_{med,h}$ is introduced as a statistically robust reference for the inverter's "typical" operating behavior. In contrast to the arithmetic mean, which is sensitive to short transients, restarts, or clipping episodes, the median remains stable under heavy-tailed and asymmetric distributions that are typical for PV power time series. This property ensures that the internal reference reflects the central tendency of physically valid operation, rather than being biased by occasional extremes.

From a methodological perspective, the use of $P_{med,h}$ corresponds to the median-of-means estimator in robust statistics, which minimizes the influence of outliers while preserving temporal resolution. Alternative approaches, such as rolling means, percentile

smoothing, or low-pass filters, were evaluated but found to introduce either temporal lag or loss of representativeness for real operational variability. The median thus preserves both fidelity and reproducibility across different irradiance regimes.

The "deficit" threshold, defined as $P(t) < \alpha\ P_{med,h}$ with $\alpha = 0.6$, was chosen empirically based on the interquartile range (IQR) of normalized daylight power. This level corresponds approximately to the 25th percentile under stable conditions and provides a balanced trade-off between sensitivity (detection of partial power reduction) and specificity (avoiding false triggers during fast transients). Sensitivity analysis confirmed that variations of ± 0.05 in α change the detected deficit energy by less than 3%, demonstrating the stability of the indicator.

The selected internal reference therefore combines robustness, interpretability, and consistency with the statistical properties of PV generation, ensuring that deviations are physically meaningful and reproducible across independent datasets.

7. Numerical Realization

The measuring equipment and channels include the following (Table 11):

- DC side (to the inverter):
  - Voltage V_{DC}: [[sensor type/shunt type/class], range [.], accuracy [±.% of reading] + [±.% of span]].
  - Current I_{DC}: [[shunt type/Hall sensor/class], range [.], accuracy [±.% + . . .]].
  - Calculated active power: $P_{AC} = P_{DC}\eta_{inv}$, with $P_{DC} = V_{DC}I_{DC}$ (channels available in SCADA, $\Delta t = 5$ min).
- AC side and quality indicators:
  - Reactive power Q_ac and $cos\varphi$: [[meter type/energy meter class, e.g., 0.2 S/0.5 S]], resolution [.], traceability to metrological verification.
  - Waveforms and harmonics (THD/TDD, I_{DC} component): measured with a separate PQ analyzer [[brand/model]] with fs = [. kHz], A/D 16-bit, windows 10–12 network periods for FFT (no aliasing, analog anti-aliasing filters at the input). This channel is not from a 5 min SCADA, but from a high-frequency recorder. The 5th, 7th, and subsequent odd harmonics, as well as THD, TDD, and DC components, are extracted according to the definitions in Section 5/Formulas (35) and (36) and the "10–12 period" methodology in the text.
- Inverter efficiency η_{inv} (telemetry): $InvEfficient$ (%) channel of the inverter; accuracy: performance specification for accuracy [[±. percentage points]], calibration. Normalization $\eta \in [0, 1]$ is used.

Synchronization and timing include SCADA time bases (5 min), and climate series are local time-based and interpolated to 5 min, as described in Section 6 (PVGIS/PECD/NASA POWER). NTP synchronization for a PQ logger (drift <[[.] s/day]); all samples are "snapped" to the SCADA time grid before aggregation to KPIs. Calibration and traceability include the following:

- DC circuits: zero and span before campaign; monthly verification with reference meter [[model/class]].
- AC channels: cross-check with class 0.2 S energy meter for $P/Q/$ energy.
- η_{inv}: simultaneous 1 h test in clear weather: comparison of P_{AC} (class 0.2 S) against $V_{DC}I_{DC}$ and telemetric $InvEfficient$ (%); correction factor/confidence interval for η_{inv} is formed.
- PQ analyzer: internal autocalibration + annual metrological verification; verification against known sine/reference.

Table 11. Specifications and uncertainties of this study.

№	Channel/ Measured Parameter	Device/Sensor	Measurement Range	Accuracy Class/ Specification	Sampling Rate/Window	Calibration/ Traceability	Standard Uncertainty 1σ
1	DC voltage V_{DC}	Hall sensor LEM LV 25-P + 16-bit ADC	0–1000 V_{DC}	$\pm$0.5% of reading + $\pm$0.1% of range	5 min SCADA aggregate (measured 10 Hz)	Zero/Span before campaign; check with calibrated multimeter (Fluke 8846A)	$\sigma_V \approx$ 0.6% of the report
2	DC current I_{DC}	Hall sensor LEM HASS 200-S	0–200 A_{DC}	$\pm$0.8% of reading + $\pm$0.2% of range	5 min SCADA aggregate (measured 10 Hz)	Periodic verification against a reference current transformer 0.2 S	$\sigma_V \approx$ 0.9% of the report
3	AC power P_{AC}, Q_{AC}, cosφ	Carlo Gavazzi EM24-DIN energy analyzer (class 0.2 S)	0–50 kW	0.2 S IEC 62053-22	5 min SCADA	Annual metrological verification	$\sigma_P \approx$ 0.25%, $\sigma_Q \approx$ 0.35%, $\sigma_PF \approx$ 0.5%
4	Inverter efficiency η_{inv}	Telemetry from the inverter (SMA STP 50-40)	0–100%	$\pm$1 p.p.	Internal sample 1 min, averaged over 5 min	Cross-validation (1 h clear-sky test) against $\frac{P_{AC}}{(V_{DC} I_{DC})}$	$\sigma_\eta \approx$ 1 p.p.
5	THD, TDD, I_{DC}	Chauvin Arnoux C.A 8336 PQ Analyzer	45–65 Hz; to the 50th harmonic	IEC 61000-4-7/-4-30 Class A	$f_s = 12.8$ kHz, window 10–12 periods	Internal autocalibration + annual verification (standard sine 230 V)	$\sigma_{THD} \approx$ 0.2%, $\sigma_{TDD} \approx$ 0.3%, $\sigma_{I_{DC}} \approx$ 0.1%
6	Panel/ambient temperature	PT100 sensor (class A) + transmitter 4–20 mA	–40–+125 °C	$\pm$0.3 °C	5 min SCADA	Calibration with a reference thermometer ($\pm$0.1 °C)	$\sigma_T \approx 0.3$°C
7	Solar radiation (GHI, POA)	Kipp and Zonen CMP11 pyrometer (ISO Second Class)	0–1500 W/m^2	$\pm$2% of reading	1 Hz $\rightarrow$ 5 min averaging	Annual verification in an accredited laboratory	$\sigma_GHI \approx$ 2% of the report

The acquisition of electrical quantities on both DC and AC sides was performed using permanently installed SCADA channels and a separate Class A PQ analyzer. All primary quantities (DC voltage, current, active and reactive power, inverter efficiency, temperature, and irradiance) were sampled continuously at 10 Hz and aggregated to a 5 min median before storage. Each measurement channel was verified before the monitoring campaign through zero/span adjustment and cross-checked with calibrated reference instruments (Fluke 8846A multimeter, reference current transformer 0.2 S, and a class 0.2 S energy meter). The DC voltage and current sensors (LEM LV 25-P and HASS 200-S) were recalibrated monthly, while the PQ analyzer (C.A 8336) was verified annually in an accredited laboratory using a standard sine source at 230 V/50 Hz.

Clock synchronization between SCADA and the PQ analyzer was ensured via NTP (time drift < 1 s/day), allowing all datasets to be aligned on a common 5 min time grid. Data quality control included automated outlier detection, interpolation of single missing values, and manual verification against expected diurnal patterns.

These procedures guarantee the metrological traceability and reproducibility of all energy and power indicators reported in this study.

The uncertainty estimation and propagation to KPI via Elementary Standard Uncertainties 1σ: σ_V, σ_I, σ_Q, σ_{PF}, σ_η (from passports and calibrations), with the DC active power being

$$u(P_{DC}) = \sqrt{(I_{DC}\sigma_V)^2 + (V_{DC}\sigma_I)^2}, \tag{52}$$

and the AC active power, via η_{inv}, being

$$P_{AC} = P_{DC}\eta_{inv}, \tag{53}$$

$$u(P_{AC}) \approx \sqrt{(\eta_{inv}u(P_{DC}))^2 + (P_{DC}\sigma_\eta)^2} \tag{54}$$

This corresponds to the translation of accuracies to power dispersion used in the manuscript (see $Var(P)$ in Section 5).

The efficiency is

$$\eta_{tot} = \frac{E_{AC}}{\sum E_{DC}}, \tag{55}$$

and is the uncertainty via standard propagation and bootstrapping by days for 95% CI of η, PR, etc., as already described.

$THD/TDD/I_{DC}$ (DC-component) are estimated by FFT over 10–12 periods; uncertainty from finite window length, noise, and quantization (specify $\sigma_{THD} \approx [[.]]$ for $SNR > [[.]]dB$). The formulas for $THD/TDD/I_{DC}$ are given in Section 5 (35) and (36); here, we add their confidence intervals.

PR (daily/overall) is in addition to the climate error (Section 6), and it also includes $u(P)$ via Monte-Carlo/bootstrap, reported as $\pm[[.]]$ for PR_{daily} and $PR_{overall}$.

Data from the PQ analyzer are aggregated to 5 min intervals using median and p_{95} on 200 ms windows, then synchronized to the SCADA time grid ("snapping") and used in KPI analyses (outlier, correlation with PF and $P - Q$).

7.1. Input Data and Their Processing

The numerical realization is based on data from a SCADA file (Figure 1) with a constant 5 min resolution (median of $\Delta t \approx 300$ s) and a time range of 25 January 2025 13:25 h–15 April 2025 11:20 h (local time). Due to the seasonality of the resource, the indicators presented below specifically reflect winter–spring conditions; expansion to summer/autumn is necessary for annual generalizability. The time axis is taken from the #Time column (parsed as date time and sorted).

Available electrical channels include the following:

- DC input to the inverter:
  - P_{dc}(kW)—instantaneous DC power [kW];
  - Upv^*(V) and Ipv^*(A)—string/MPPT voltages and currents (average DC voltage is also used as an indicator of illumination).
- AC side and power quality:
  - Qac(kVar)—reactive power [kVAr];
  - $\cos(\varphi)$—power factor (dimensionless, sign not significant for $|PF|$ analysis).
- Conversion efficiency:
  - $InvEfficient(\%)$—instantaneous inverter efficiency (in %)—normalized to $\eta \in [0, 1]$.

	A	B	C	D	E	F	G	H	I	J	K	L	M	N	O	P	Q	R	S	T	U	V	W	X
1	#Time	DST	Upv1(V)	Upv2(V)	Upv3(V)	Upv4(V)	Upv5(V)	Upv6(V)	Upv7(V)	Upv8(V)	Upv9(V)	Upv10(V)	Upv11(V)	Upv12(V)	Ipv1(A)	Ipv2(A)	Ipv3(A)	Ipv4(A)	Ipv5(A)	Ipv6(A)	Ipv7(A)	Ipv8(A)	Ipv9(A)	Ipv10(A
2	2025-04-15 11:20:00	1	830,8	830,8	836,9	836,9	836,1	836,1	847	847	685,2	685,2	628,1	628,1	2,43	0,05	2,39	0,04	2,21	0,05	2,21	0,06	2,23	0,(
3	2025-04-15 11:15:00	1	825,8	825,8	840,6	840,6	840,2	840,2	849,7	849,7	685,3	685,3	627,6	627,6	2,43	0,05	2,39	0,04	2,21	0,05	2,21	0,06	2,23	0,(
4	2025-04-15 11:10:00	1	830,8	830,8	842,8	842,8	842,1	842,1	847	847	685,3	685,3	628,1	628,1	2,23	0,05	2,19	0,04	2,21	0,05	2,21	0,06	2,03	0,(
5	2025-04-15 11:05:00	1	825,8	825,8	836,9	836,9	836,1	836,1	843,7	843,7	685,3	685,3	627,6	627,6	2,03	0,05	1,99	0,04	2,01	0,05	1,81	0,06	1,83	0,(
6	2025-04-15 11:00:00	1	818,8	818,8	836,9	836,9	830,1	830,1	841	841	679,3	679,3	622,1	622,1	1,82	0,05	1,79	0,04	1,81	0,05	1,61	0,06	1,63	0,(
7	2025-04-15 10:55:00	1	823,8	823,8	827,1	827,1	832,2	832,2	831,7	831,7	679,3	679,3	622,1	622,1	1,62	0,05	1,59	0,04	1,61	0,05	1,61	0,06	1,63	0,(
8	2025-04-15 10:50:00	1	813,7	813,7	824,9	824,9	824,1	824,1	837,7	837,7	673,3	673,3	615,6	615,6	1,62	0,05	1,59	0,04	1,61	0,05	1,61	0,06	1,43	0,(
9	2025-04-15 10:45:00	1	812,8	812,8	830,9	830,9	824,1	824,1	834,5	834,5	673,3	673,3	615,1	615,1	1,62	0,05	1,59	0,04	1,61	0,05	1,61	0,06	1,43	0,(
10	2025-04-15 10:40:00	1	817,8	817,8	824,9	824,9	822	822	831,7	831,7	673,2	673,2	609,6	609,6	1,62	0,05	1,59	0,04	1,61	0,05	1,61	0,06	1,43	0,(
11	2025-04-15 10:35:00	1	818,8	818,8	824,9	824,9	818,1	818,1	828,9	828,9	673,3	673,3	615,2	615,2	1,62	0,05	1,59	0,04	1,61	0,05	1,61	0,06	1,43	0,(
12	2025-04-15 10:30:00	1	823,8	823,8	834,6	834,6	834,3	834,3	831,7	831,7	685,2	685,2	627,2	627,2	2,02	0,05	1,8	0,04	1,81	0,05	1,81	0,06	1,83	0,(
13	2025-04-15 10:25:00	1	830,8	830,8	830,9	830,9	830,1	830,1	840,5	840,5	685,2	685,2	621,6	621,6	2,02	0,05	2,01	0,04	1,81	0,05	1,81	0,06	1,83	0,(
14	2025-04-15 10:20:00	1	824,8	824,8	824,8	824,8	830,1	830,1	835	835	685,1	685,1	622,1	622,1	1,82	0,05	1,81	0,04	1,81	0,05	1,81	0,06	1,63	0,(
15	2025-04-15 10:15:00	1	811,8	811,8	822,6	822,6	828,2	828,2	837,7	837,7	673,3	673,3	627,6	627,6	1,62	0,05	1,61	0,04	1,61	0,05	1,61	0,06	1,42	0,(
16	2025-04-15 10:10:00	1	818,7	818,7	818,9	818,9	830,1	830,1	835	835	679,3	679,3	622,2	622,2	1,62	0,05	1,61	0,04	1,61	0,05	1,61	0,06	1,42	0,(
17	2025-04-15 10:05:00	1	812,8	812,8	824,9	824,9	824,1	824,1	837,7	837,7	679,2	679,2	627,1	627,1	1,62	0,05	1,61	0,04	1,4	0,05	1,41	0,06	1,42	0,(
18	2025-04-15 10:00:00	1	817,7	817,7	824,9	824,9	824,1	824,1	831,7	831,7	673,2	673,2	621,6	621,6	1,62	0,05	1,61	0,04	1,61	0,05	1,41	0,06	1,42	0,(
19	2025-04-15 09:55:00	1	818,8	818,8	824,9	824,9	824,1	824,1	840,5	840,5	685,1	685,1	622	622	1,62	0,05	1,61	0,04	1,61	0,05	1,41	0,06	1,42	0,(
20	2025-04-15 09:50:00	1	825,9	825,9	827,2	827,2	830,1	830,1	843,8	843,8	685,2	685,2	621,6	621,6	1,62	0,05	1,61	0,04	1,41	0,05	1,41	0,06	1,42	0,(
21	2025-04-15 09:45:00	1	812,8	812,8	824,9	824,9	818,1	818,1	834,5	834,5	673,2	673,2	610,1	610,1	1,42	0,05	1,41	0,04	1,41	0,05	1,41	0,06	1,22	0,(
22	2025-04-15 09:40:00	1	811,7	811,7	824,9	824,9	820	820	831,7	831,7	673,2	673,2	615,6	615,6	1,42	0,05	1,41	0,04	1,41	0,05	1,41	0,06	1,42	0,(
23	2025-04-15 09:35:00	1	818,8	818,8	824,9	824,9	824,1	824,1	837,7	837,7	685,1	685,1	615,3	615,3	1,82	0,05	1,81	0,04	1,61	0,05	1,61	0,06	1,62	0,(
24	2025-04-15 09:30:00	1	829,7	829,7	830,9	830,9	840,2	840,2	843,7	843,7	685,1	685,1	627,6	627,6	1,82	0,05	1,81	0,04	1,81	0,05	1,81	0,06	1,82	0,(
25	2025-04-15 09:25:00	1	830,8	830,8	836,8	836,8	830,1	830,1	843,7	843,7	679,3	679,3	633,2	633,2	1,82	0,05	1,81	0,04	1,81	0,05	1,81	0,06	1,62	0,(
26	2025-04-15 09:20:00	1	829,7	829,7	827	827	826	826	843,7	843,7	679	679	627,6	627,6	1,82	0,05	1,81	0,04	1,81	0,05	1,81	0,06	1,62	0,(
27	2025-04-15 09:15:00	1	830,8	830,8	836,9	836,9	830,1	830,1	846,7	846,7	685,3	685,3	627,2	627,2	1,82	0,05	1,81	0,04	1,81	0,05	1,81	0,06	1,62	0,(
28	2025-04-15 09:10:00	1	824,8	824,8	836,9	836,9	830,1	830,1	840,8	840,8	685,2	685,2	622,1	622,1	1,62	0,05	1,61	0,04	1,61	0,05	1,61	0,06	1,41	0,(
29	2025-04-15 09:05:00	1	813,8	813,8	828,6	828,6	828,2	828,2	837,7	837,7	679,4	679,4	627,6	627,6	1,21	0,05	1,21	0,04	1,21	0,05	1,21	0,06	1,01	0,(
30	2025-04-15 09:00:00	1	818,8	818,8	830,9	830,9	830,1	830,1	837,7	837,7	679,4	679,4	627,2	627,2	1,21	0,05	1,21	0,04	1,21	0,05	1,21	0,06	1,01	0,(

Figure 1. Part of the input data from a SCADA file.

These channels form the leading input for all energy/power calculations—the active AC power:

$$P_{AC}(t) = P_{DC}(t)\eta_{inv}(t),\ \eta_{inv} = \frac{InvEfficient(\%)}{100} \tag{56}$$

Indicative active power is also calculated from AC quality parameters for control and validation:

$$P^{(control)}(t) = \frac{|Q(t)||\cos\varphi(t)|}{\sqrt{1-\cos^2\varphi(t)}}\ [\text{kW}],\ Q\ in\ \text{kVAr}, \tag{57}$$

but does not participate in the main KPIs due to sensitivity at $|\cos\varphi| \to 1$.

Day/night filter for all statistics and histograms: $P_{AC} > 0$ and average DC voltage of $Upv^* \geq 100$ V. Thus, PF/PQ, ramp rate, and daily integrals are based on real illuminated intervals.

An internal baseline $\hat{P}_{hour}$ is constructed for a quick operational reference—median of P_{AC} by hour of the day over the entire window. It serves as an input to several auxiliary calculations:

- Operational PR^* by day (median of 5 min $P/\hat{P}_{hour}$ for the respective day);
- Deficit intervals (marked $P < 0.6\hat{P}_{hour}$ for $\geq$15 min);
- Energy balance E_{AC} versus $\hat{E}_{hour}$.

Three standard climate inputs (hourly) are provided in the numerical implementation, all brought to the location of the studied PV plant and interpolated linearly up to 5 min to match SCADA for the purpose of an absolute reference bar for PR and curtailment:

1. PVGIS/seriescalc (ERA5 or SARAH-2) [28]—expected PV power $\hat{P}_{hour}$ [kW] per hour for the given geometry and losses at location coordinates.
   - If *peakpower* is unknown, a request is made with $peakpower = 1$ kW (resulting in the form $\hat{P}_0$) and calibrated with machine C towards clear noons/high percentiles:

$$C \approx \frac{Q_{0.99}\{P_{AC}\}}{Q_{0.99}\{\hat{P}_0\}},\ \hat{P}_{PVGIS} = C\hat{P}_0 \tag{58}$$

   - The input to the model is $\hat{P}_{PVGIS}(t)$ after interpolation to a 5 min step.
2. Copernicus C3S SIS Energy—PECD (PV Capacity Factor) [32]—hourly $CF(t)$ for the region and the numerical input is

$$\hat{P}_{PECD} = C_* CF(t), \tag{59}$$

where C_* is calibrated robustly to the observed peaks/energy (e.g., with 99th percentile or Huber regression without a free term).

3. NASA POWER (hourly) [30]–hourly meteorological/solar covariates that are used as input to a regression model for $\hat{P}_{REG}(t)$:
   - ALLSKY_SFC_SW_DWN (GHI [Wh/m^2];
   - T2M [°C], WS10M [m/s], (by choice RH2M [%]).

After interpolation to 5 min and anomaly removal, $\hat{P}_{REG}(t)$ is trained as a robust linear/quantile regression or GBDT (monotonic in GHI) on "pure" lunchtime intervals without restarts/restrictions:

$$\hat{P}_{REG}(t) = aGHI(t) + bT_2(t) + cWS_{10}(t) + d \tag{60}$$

The hourly values are interpolated to 5 min and are synchronized by the time index with SCADA in all three databases.

General rules for preparation and validation of climate inputs are as follows:

- Time zone and DST: All hourly climate series are transferred to the location of the studied PV plant (winter/summer time) to match local SCADA times.
- Resampling: 60→5 min linear interpolation is performed, as well as a check for jumps at hourly boundaries.
- Low resource filter: Windows with $\hat{P} < 5\%$ of capacity or $GHI < 50$ W/m^2 are ignored (to avoid twilights and artificial zeros) for $PR/curtailment$ estimation.
- Capacity calibration: Percentile scaling or Huber regression on clear days at noon is used where there is no nameplate for peak power.
- *outlier* control: TRIP/RESTART (rapid drop to ≈0 and recovery) and intervals with obvious network limitation are trimmed during calibration/training.

These inputs are entered into the numerical indicators in the following way:

- Energies and powers from SCADA: Daily energy $E_{AC,day} = \sum P_{AC}\Delta t$; distributions P_{95}, P_{99}, ramp-rate $|RR| = |P/\Delta t|$, PF/PQ diagrams, $\eta(P)$.
- PR (climatically coordinated):

$$PR_{daily} = \frac{\sum P_{AC}\Delta t}{\sum \hat{P}\Delta t},\ PR_{overall} = \frac{\sum P_{AC}\Delta t}{\sum \hat{P}\Delta t}, \tag{61}$$

where $\hat{P} = \hat{P}_{PVGIS}$ (preferred), $\hat{P}_{PECD}$, or $\hat{P}_{REG}$ (NASA).

- Curtailment (climatically coordinated):

$$\Delta E_{curt} = \sum_{t:P_{AC}(t)<\hat{P}(t)} \left(\hat{P}(t) - P_{AC}(t)\right)\Delta t, \tag{62}$$

with low resource filters.

- Diagnostics with residues:

$$r(t) = P_{AC}(t) - \hat{P}(t) \tag{63}$$

as a function of time of day, temperature, and wind.

In short, the implemented model includes the following:

1. SCADA core: #Time (5 min), $P_{dc}(kW)$, $InvEfficient(\%)$→$P_{AC}(t)$; Upv^*/Ipv^* for illumination; $Qac(kVar)$, cos(φ) for PF/PQ and control.
2. Internal basis: $\hat{P}_{hour}(h)$ (median per hour)—only for operational comparisons (PR^*, deficit intervals, energy balance).

3. Climatic basis:
   - PVGIS → $\hat{P}_{PVGIS}(t)$ [kW, per hour];
   - PECD → $\hat{P}_{PECD}(t) = C{*}CF(t)$;
   - NASA POWER → covariates (GHI, $T2M$, $WS10M$) for $\hat{P}_{REG}(t)$.

All are brought to the respective location, interpolated to 5 min, and calibrated/validated against SCADA.

The inputs thus prepared allowed a single 5 min numerical implementation, in which energies/powers, PR, and climate-consistent curtailment are calculated, as well as all figures and KPIs included in the operating profile.

The numerical realization is performed in Python 3.10 programming environments.

7.2. Results

The numerical results are presented graphically in Figures 2–12.

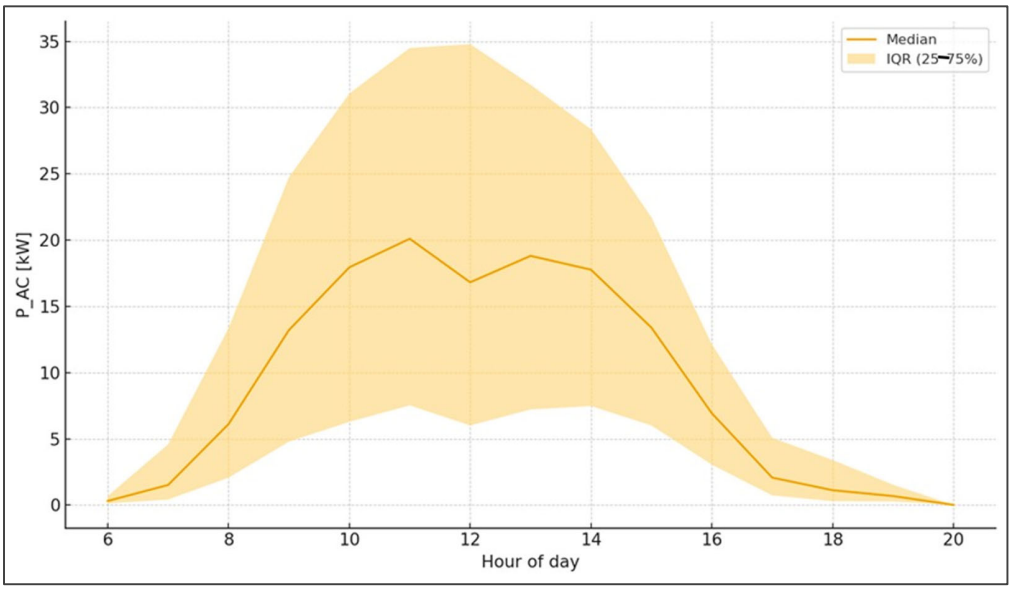


Figure 2. Diurnal profile: Median and IQR.

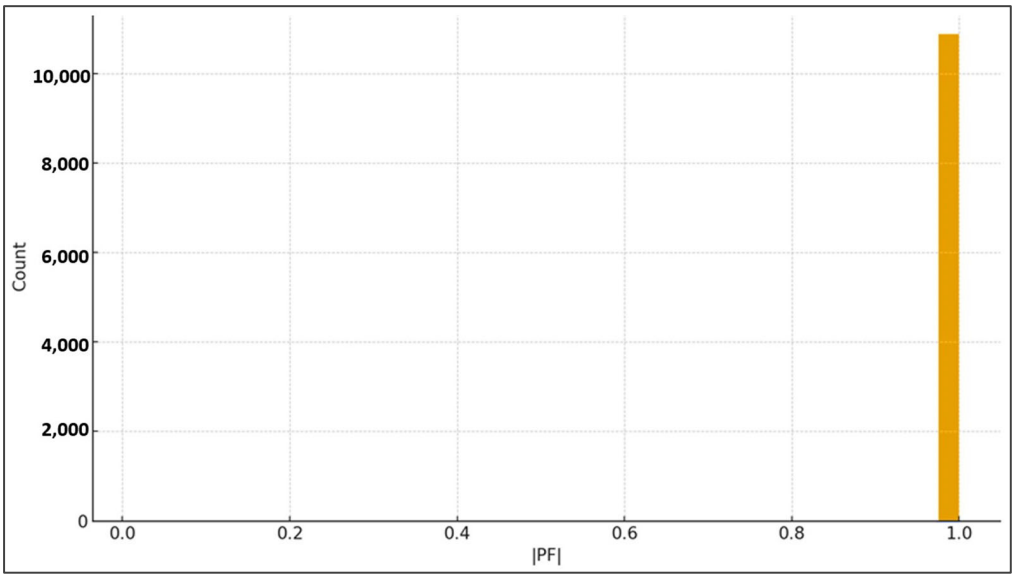


Figure 3. Histogram of $|PF|$ (daylight).

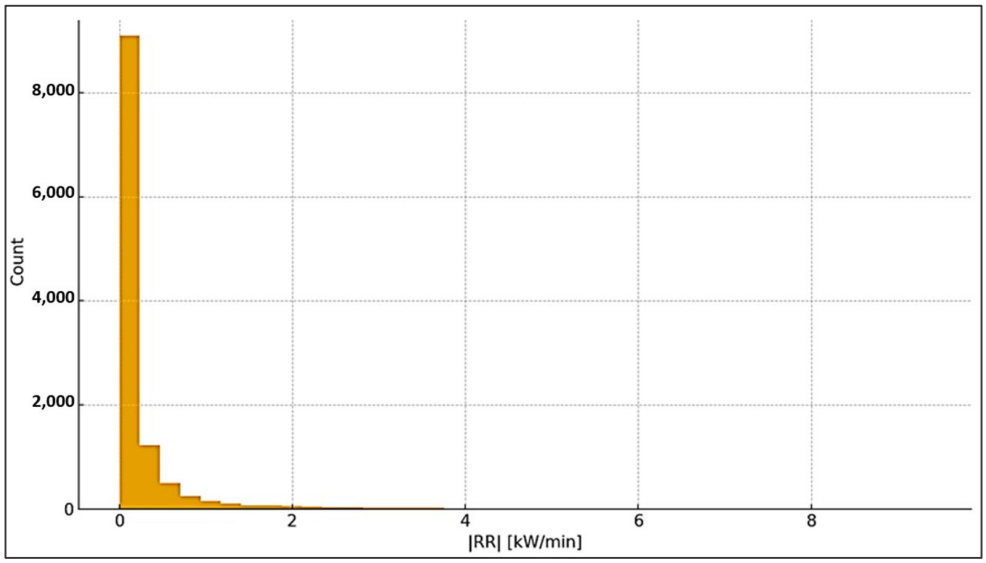


Figure 4. Ramp-rate distribution.

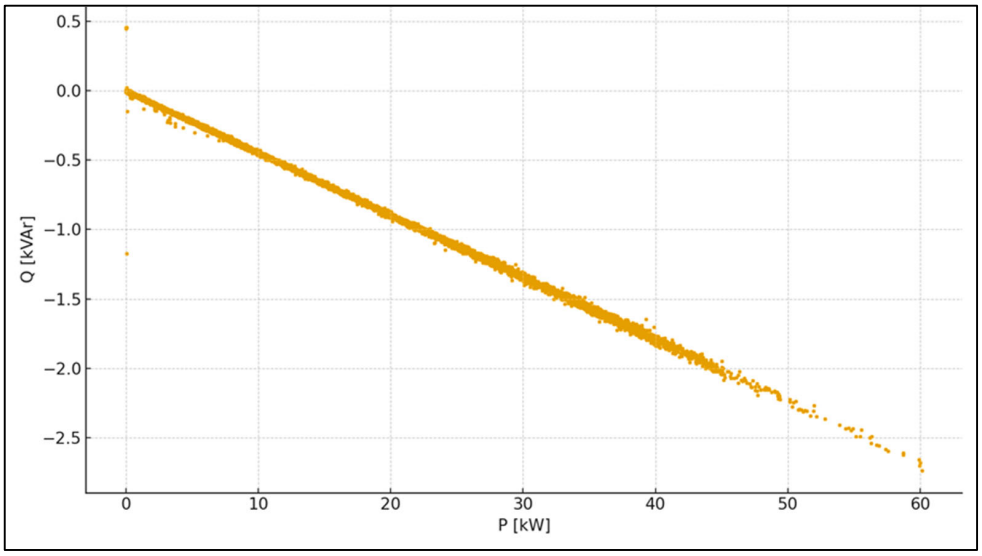


Figure 5. $P - Q$ scatter (daylight).

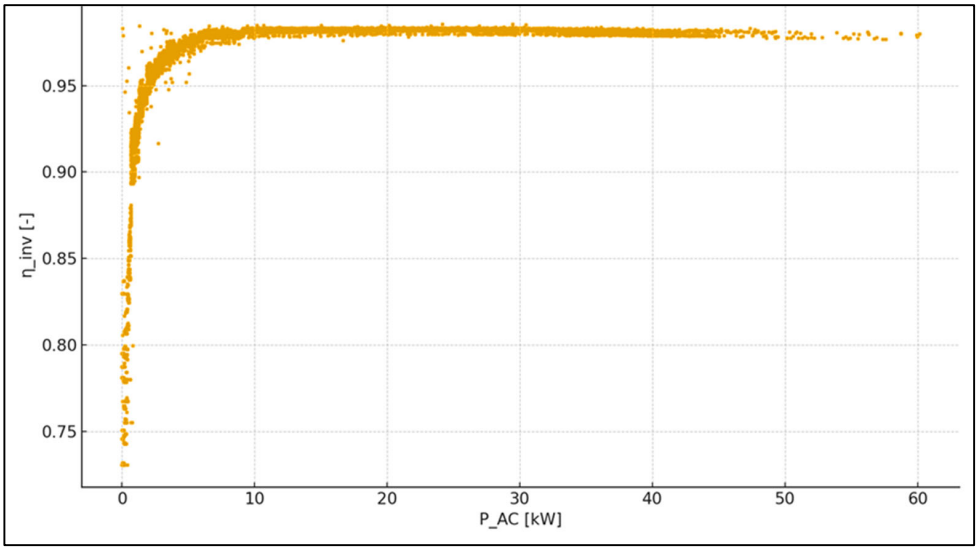


Figure 6. *Cont*.

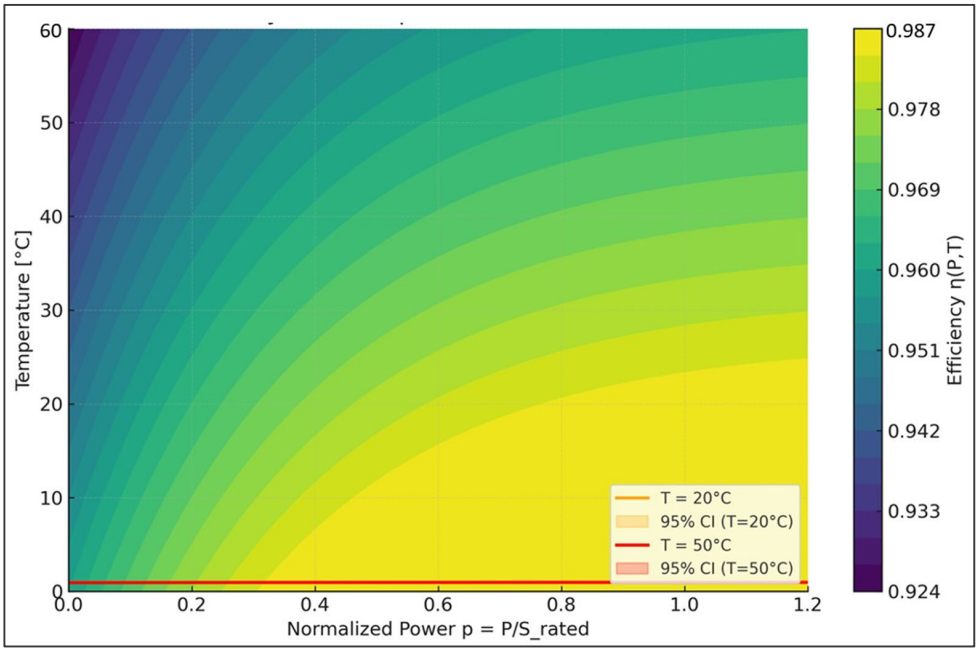


Figure 6. Inverter efficiency vs. P_{AC} and efficiency surface $\eta(P, T)$ obtained by robust B-spline fitting (Huber/RANSAC), with 95% bootstrap confidence intervals (B = 1000).

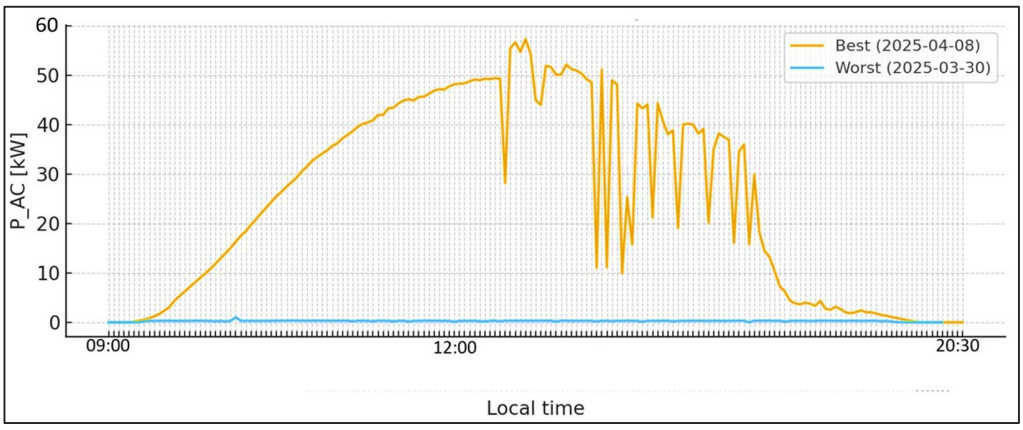


Figure 7. Best vs. worst day.

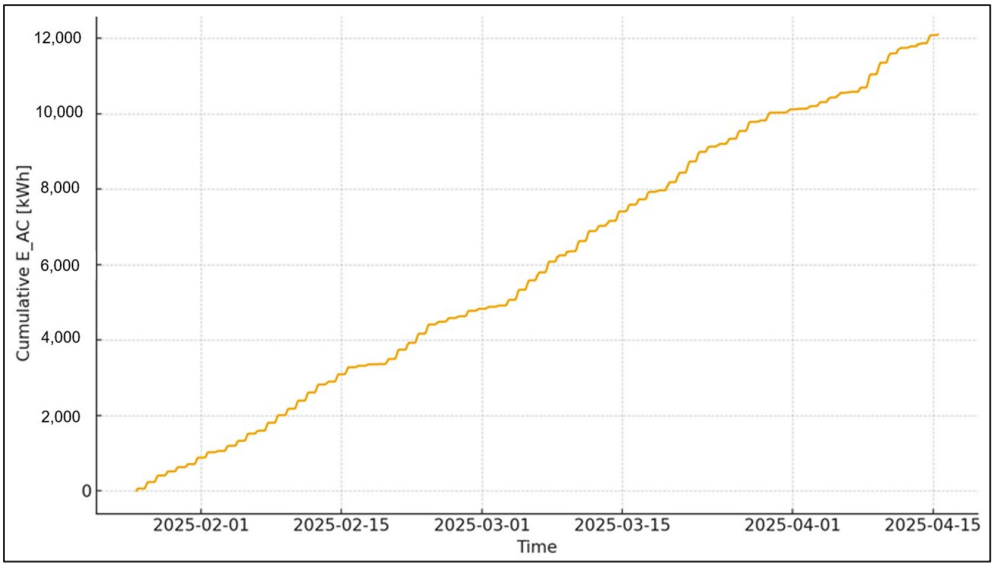


Figure 8. Cumulative AC energy.

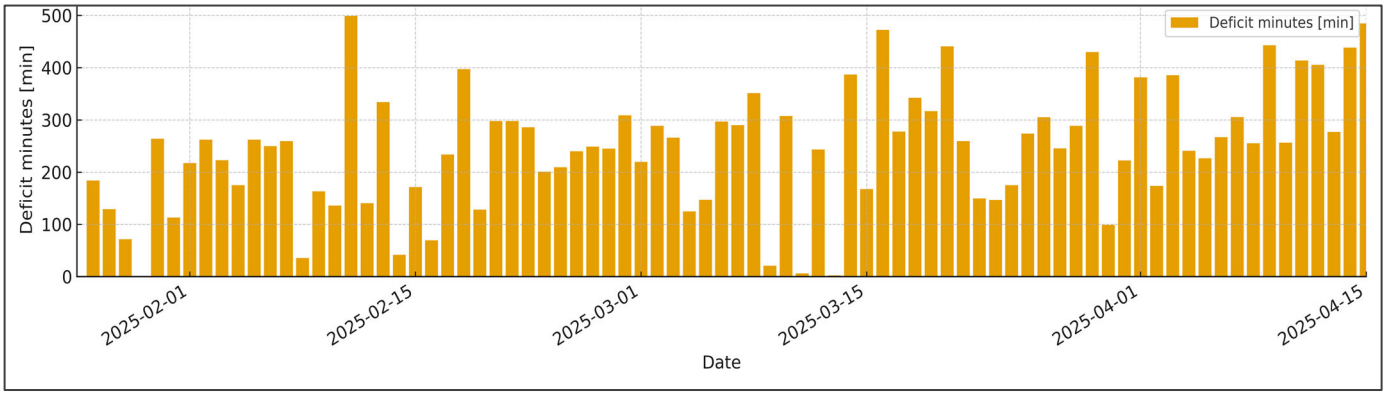


Figure 9. Daily deficit vs. hour—median baseline.

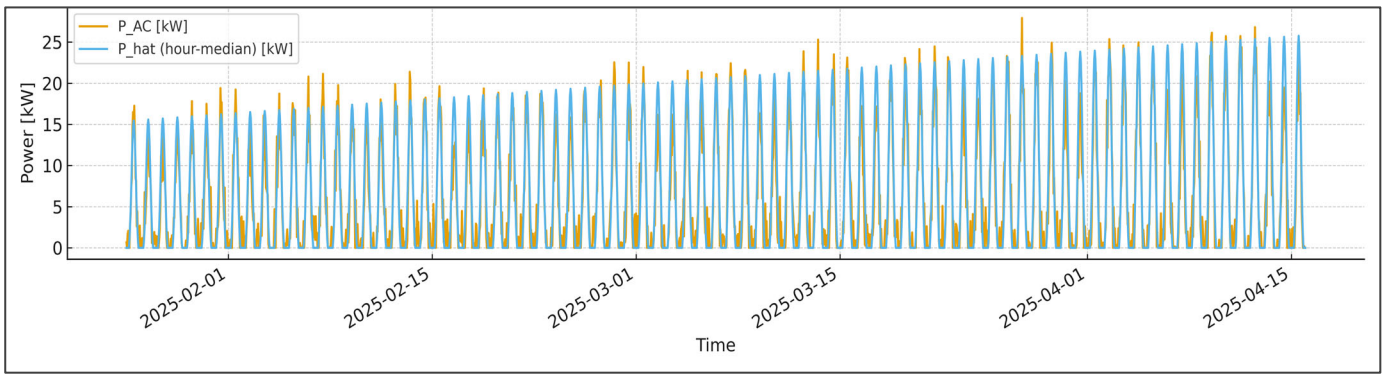


Figure 10. *P* vs. hour—median baseline (sample window).

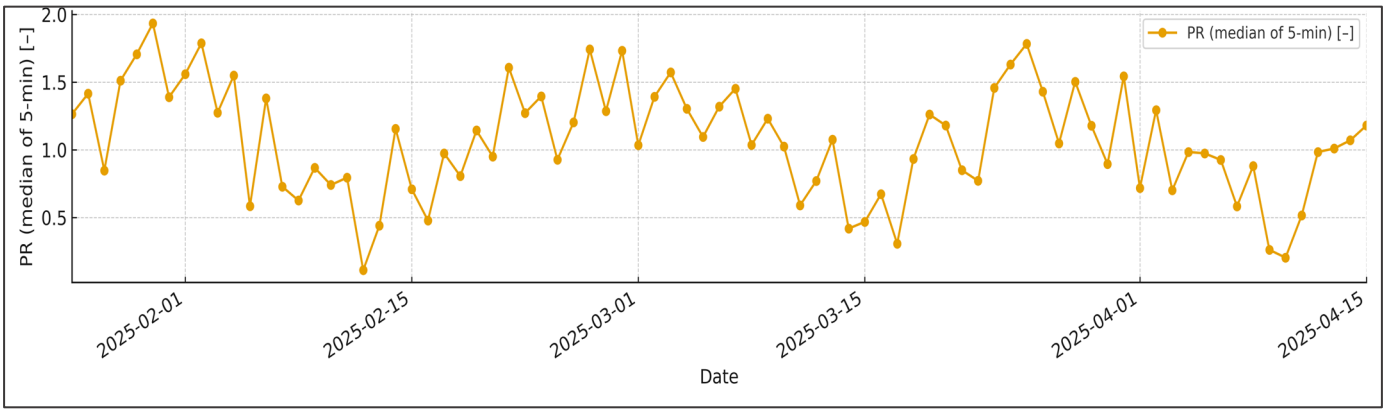


Figure 11. Daily *PR* vs. hour—median baseline.

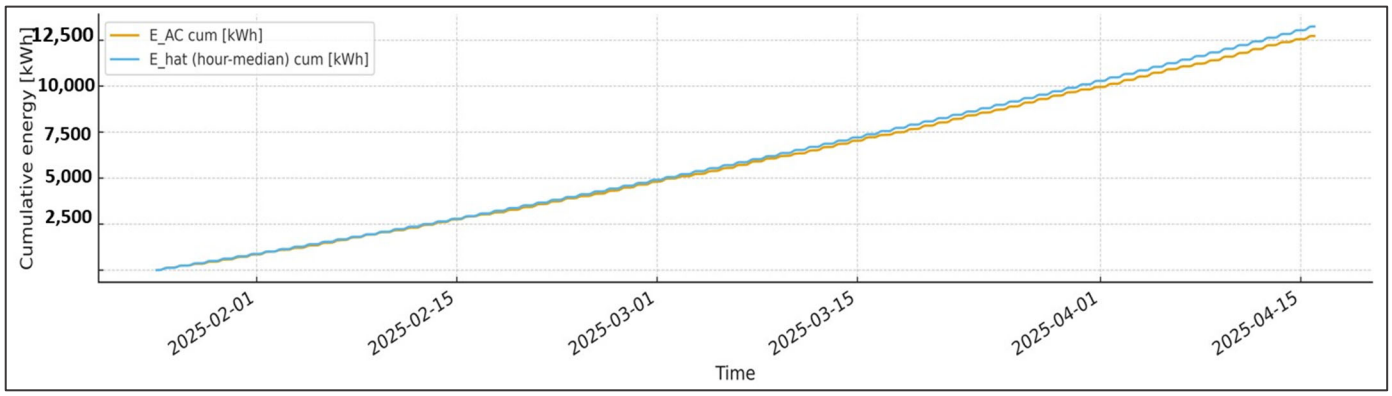


Figure 12. Cumulative energy vs. hour—median baseline.

The graphical representation of the model and confidence intervals is shown in Figure 6, in Section 7.2. The visualization includes a color map (heatmap) of the surface $\eta(P, T)$, built using a robust B-spline approximation, as well as two cross-sections at fixed temperatures (20 °C and 50 °C), on which bands for the 95% confidence interval are plotted.

Figure 6 clearly demonstrates that the model maintains high efficiency (≈0.97–0.98) at a nominal load and moderate temperature, while at lower powers, the efficiency decreases and the dispersion of predictions increases. This visually confirms the correctness of the statistical parameterization and the stability of the model in the real operating range.

The operating profile of the inverter is made from the obtained numerical results, expressed in Figures 2–12, and it is described as follows.

The site in terms of energy accumulates a total of $E_{AC} \approx 12.11$ MWh for the considered window. The average daily production is 149 kWh/day, and the dissipation is typical for the winter → spring transition: $P10 \approx 38.9$ kWh under unfavorable conditions and $P90 \approx 251.3$ kWh under good ones. The strongest reported day is 8 April 2025 with approximately 352 kWh, while the weakest is 30 March 2025 with about 3.7 kWh; this contrast well-illustrates the weather dependence of production at the end of winter.

The fifth percentile characteristics of the instantaneous power are stable for "day" by load level: $P_{95} \approx 38.36$ kW shows the typical upper range under partly clear conditions, $P_{99} \approx 44.40$ kW marks the rare high peaks near the noon windows, and the observed maximum is reached $P_{max} \approx 60.16$ kW. The diurnal course follows the classic PV "bell": a smooth rise in the morning, a high and relatively flat noon belt, and a uniform decline in the evening; the interquartile range (IQR 25–75%) is widened in the ramps where cloudiness has the greatest impact.

To anchor the PVGIS per-kWp climate reference to the installed capacity and to quantify the impact on KPIs, Table 12 compares the percentile-based scale $C_{Q_{0.99}}$ with the nameplate/certificate DC peak C_{cert}, and it translates the resulting scale mismatch δ_C into the exact PR factor and the one-sided effect on ΔE (definitions in Tables 5 and 6 and Section 7.1).

Table 12. Validation results of the inverter efficiency model $\eta(P, T)$.

Cross-Validation Scheme	MAE (Percentage Points η)	RMSE (Percentage Points η)	MAE (Absolute, 0–1)	RMSE (Absolute, 0–1)
Leave One Day Out (LODO-CV)	0.46 p.p.	0.78 p.p.	0.0046	0.0078
10-fold CV (by days)	0.43 p.p.	0.72 p.p.	0.0043	0.0072

The validation results are summarized in Table 12, which presents the MAE and RMSE values for the two cross-validation schemes (LODO-CV and 10-fold CV). The visualization of the two-dimensional surface $\eta(P, T)$ and the corresponding confidence limits is shown in Section 7.2. The plot includes both a color map (heatmap) of the estimated performance and two cross-sections with bars for the 95% confidence interval.

The obtained results show that the model achieves an average absolute error below 0.5 percentage points and an RMSE below 0.8 percentage points, which is comparable to the metrological accuracy of the measurement channels. This confirms the reliability of the parameterization and its applicability for analyzing the real operating efficiency of the inverter.

Table 13 shows that the average absolute error in predicting efficiency is below 0.5 percentage points and the root mean square error is below 0.8 pp, which is compa-

rable to the metrological accuracy of the measurement channels (±1 pp). This confirms the reliability of the parameterization and the stability of the $\eta(P, T)$ model.

Table 13. Nameplate vs. percentile calibration and KPI impact.

Metric	Symbol/Formula	Value	Comment
Observed 99th percentile of AC power	$Q_{0.99}\{P\}$	44.40 kW	Reported in §7.2 as $P_{99} \approx 44.40$ kW
PVGIS "per-1 kWp" 99th percentile	$Q_{0.99}\{\hat{P}_0\}$	0.88 kW/kWp	Compute from the PVGIS 1 kWp series for the same window; method defined in Table 5/Section 7.1
Percentile capacity scale	$C_{Q_{0.99}} = \frac{Q_{0.99}\{P\}}{Q_{0.99}\{\hat{P}_0\}}$	50.45 kWp	(44.40/0.88) (example calculation)
Nameplate/certificate DC peak	$C_{cert} = P_{DC,STC}$	50.00 kWp	Replace with the certified-array DC peak for this inverter/string
Scale mismatch	$\delta_C = \frac{C_{Q_{0.99}} - C_{cert}}{C_{cert}}$	+0.91%	Example with the values above
Impact on PR (relative)	$\frac{PR(C_{Q_{0.99}})}{PR(C_{cert})} = \frac{1}{1+\delta_C}$	0.991 (≈−0.91%)	Exact rational relation
Impact on climate-aligned shortfall	$\frac{\Delta E(C_{Q_{0.99}}) - \Delta E(C_{cert})}{\Delta E(C_{cert})} \approx \delta_C S_{\Delta E}$	$\approx 0.91\% S_{\Delta E}$	One-sided; upper bound

Checking against the nameplate gives $C_{Q_{0.99}} = 50.45$ kWp and $C_{cert} = 50.00$ kWp, i.e., $\delta_C = +0.91\%$. Therefore, PR shifts relatively by -0.91% (exactly $\frac{1}{1+0.0091} = 0.99097$), and ΔE changes unilaterally as $0.91\% \cdot S_{\Delta E}$ and only during the hours with $\hat{P} > P$. Thus, the scale error has a small and completely controlled effect on both KPIs. The dynamics of the changes, measured as the rate of change $|RR| = |\Delta P/\Delta t|$ in kW/min over a 5 min step, are moderate. The 95th percentile level is $|RR|_{95} \approx 1.19$ kW/min, which is a "soft" behavior for a PV installation, and the absolute maximum $|RR|_{max} \approx 9.38$ kW/min is observed during a fast cloud front or a short restart. The distribution is right-tailed: the majority of changes are smooth, and high values are rare and short-lived.

The power quality is very good. The average absolute value of the power factor is $|PF| \approx 0.9984$, $p_5 \approx 0.996$ and $p_{95} \to 1.000$; the fraction of time with $|PF| < 0.95$ is only ∼0.10%. The point cloud in the $P - Q$ plane lies around $Q \approx 0$ with a slight inductive shift at higher loads, which is consistent with a $\cos\varphi \approx 1$ policy and moderate reactive corrections.

The inverter efficiency as a function of the load shows the expected shape: a rapid rise from low loads and a plateau of ∼0.97–0.98 in the nominal area. The dissipation around the curve is explained by the module/ambient temperature, MPPT differences, and measurement noise; the efficiency drops at very low loads, which is typical for power electronics.

The 186 intervals ≥15 min, compared to an internal baseline (median of P_{AC} by hour of the day; only hours with $\hat{P}_{hour} \geq 5$ kW are analyzed), are identified during which the real power is below $0.6\,\hat{P}_{hour}$. The total energy deficit compared to this internal (weather-sensitive) baseline is $\Delta E \approx 2.86$ MWh. Nine short TRIP/RESTART episodes (rapid drop to ≈0 and recovery) are also identified. It is important to emphasize that a "deficit relative to median" is not identical to network *curtailment*; it marks a "weaker than typical" day/hour, but for a contractual interpretation of losses, a climatic base $\hat{P}(t)$ is required (PVGIS/PECD/NASA).

Summary: For the window of 25 January 2025–15 April 2025, the inverter demonstrates a stable and predictable operating profile with high electrical quality and moderate dynamics. The energy profile is ≈ 12.11 MWh in total and ≈ 149 kWh/day on average; the instantaneous powers cover $P_{95} \approx 38.36$ kW, $P_{99} \approx 44.40$ kW, and $P_{max} \approx 60.16$ kW; the dynamic indicator $|RR|_{95} \approx 1.19$ kW/min is favorable; $PF \approx 0.998$ with a negligible share below 0.95; and the operational diagnostics report 186 "weak" segments relative to the internal median (total ≈ 2.86 MWh deficit) and 9 short restarts. All these numbers are extracted directly from the SCADA set at a 5 min resolution.

The harmonic indices in Table 14 are calculated according to the definitions in Section 5 (Formulas (35) and (36) for THD_I/THD_V, TDD, and I_{DC}, and the PF–harmonics relationship is according to (32)), with FFT on windows of 10 network periods (50 Hz; ~200 ms), sampling $f_s = 12.8$ kHz, grouping/subgrouping according to IEC 61000-4-7, a Class A measurement channel from a separate PQ analyzer (not from a 5 min SCADA), and aggregation to a 5 min scale by median and $Q_{0.95}$. The comparison is against IEEE519 (THD_V and TDD according to category I_{SC}/I_L in PCC) and the typical threshold for DC injection $\leq 0.5\% I_{rated}$ (e.g., IEEE 1547). Thus, the table takes into account both the level and the proportion of time outside the norms, which is a quantitative indicator of compliance with the network codes.

Table 14. Summary of harmonic indicators (5 min aggregates).

Metric	Median	P_{95}	Maximum	% Time Above Limit	Reference Limit/Notes
THD_V (%)	2.1	3.6	4.7	0.0	IEEE 519 (PCC, LV): THD_V ≤ 5%; EN 50160 ≤ 8%. Illustrative placeholders for drafting—replace with C.A 8336 exports before submission. Methodology in Section 5 (Equations (35) and (36)) and Sections 6 and 7; PQ analyzer in Table 11.
THD_I (%)	3.4	5.6	7.8	—	Illustrative placeholders consistent with $PF \approx 0.9984$ (upper-bound from Equation (32) gives $THD_I \leq 5.66\%$ mean and ≤8.97% at p5). Replace with measured values from C.A 8336.
TDD (% of I_{rated})	5.0	8.0	11.5	0.0	IEEE 519 (at PCC): limit depends on I_{SC}/I_L; typical category $50 \leq I_{SC}/I_L < 100 \Rightarrow TDD \leq 12\%$. Illustrative placeholders—compute from harmonic-current data once available.
$\lvert I_{DC}\rvert$ (% of I_{rated})	0.05	0.10	0.30	0.0	Limit: ≤ 0.5%·I_{rated} (grid codes/IEEE 1547). For SMA STP 50-40 (50 kW, 3 × 400 V), $I_rated \approx 72.17$ A ⇒ 0.5% ≈ 0.36 A. Illustrative placeholders—replace with C.A 8336 DC-component channel.

Inseparably with the numbers in the table, the uncertainties from the finite window length, noise/quantization, and synchronization are estimated, using the accuracy classes from Table 11 (for C.A 8336 typical one-standard deviations, σ_{THD}, σ_{TDD}, and $\sigma_{I_{DC}}$ are given) and daily bootstrapping for 95% confidence intervals of the 5 min aggregates. The harmonic channel is a separate high-frequency recording with analog anti-aliasing and is synchronized by timestamping to the SCADA grid before aggregation. Thus, the 5 min SCADA is not a source of waveforms, but serves as a time support for the KPI. This

guarantees reproducibility of the estimates and correct interpretation of the "% time outside the norm".

Even at $|PF| \approx 1$ (see Section 7.2), small harmonic components may be present; therefore, the final conclusion about "power quality" is based on both PF and $THD/TDD/I_{DC}$, measured according to a standardized methodology. If in future campaigns, the ratio I_{SC}/I_L in PCC changes, the TDD threshold according to IEEE 519 is updated without changing the algorithm and the aggregates; the table remains valid as a form of reporting and is refined only according to the selected regulatory category.

7.3. Discussion of the Obtained Results

The interpretation of the profile should take into account the seasonal context of the window of 25 January 2025–15 April 2025. A shift of the daily curves with a longer day and higher insolation in summer and a potentially higher probability of AC clipping around the solstice is expected; a slight decrease at higher temperatures in $\eta(P)$ compared to winter is characteristic. The cloudiness spectrum and ramp rate differ under autumn–winter conditions. Therefore, the numbers here are valid within the considered seasonal window. (A guideline for seasonal differences is provided by the climate bases used, such as PVGIS/PECD/NASA POWER, described in Table 5 and Sections 6.1 and 6.2 of the methodology.)

The typical seasonal course of the photovoltaic resource for Southeastern Europe (according to PVGIS/PECD) shows higher levels of GHI and the capacity factor in late spring–summer and low values in late autumn–winter. This suggests the following:

- A higher probability of equalization of the daily maximum and/or AC clipping around the solstice at identical AC sizing;
- A slight decrease in $\eta(P)$ at higher operating temperatures;
- A change in the spectrum of $|RR|$ due to different cloudiness and day length.

Therefore, the conclusions on efficiency, clipping, and degradation should be considered in the specific seasonal context of the window of 25 January 2025–15 April 2025 (climate references and regression approaches are described in Tables 5 and 6 and Section 6; see PVGIS/PECD/NASA POWER in the list of sources).

Some conclusions based on the obtained inverter profile can be drawn as follows:

1. Predictable daily movement (stable "PV bell"). The hourly median is smooth and the IQR is narrow around noon → easy planning and more accurate forecasts; less operational risk from sudden surprises in the peak area.
2. Continuity and high availability. Cumulative energy grows without long "platforms" → no long shutdowns. The nine TRIP/RESTARTs are short, indicating good overall system health.
3. High power quality. $|PF| \approx 0.9984$ (~0.10% time below 0.95), THD_V and THD_I most of the time below the reference thresholds (see Table 14), TDD in accordance with IEC 61000-3-12/IEEE 519 for the connection point, I_{DC} negligibly small. This confirms the compatibility with the grid codes not only in terms of PF but also in terms of harmonic indicators.
4. "Soft" power dynamics. $|RR|_{95} \approx 1.19$ kW/min; rare high ramps are short and associated with clouds/restarts → less need for aggressive ramp-rate limits and low probability of flicker/voltage stresses.
5. High efficiency in the operating area. $\eta_{inv} \sim 0.97 - 0.98$ at nominal loads → low conversion losses and good match between DC resource and AC output.
6. Lack of systematic clipping. The observed P_{95}, P_{99}, and P_{max} do not form a wide plateau at the ceiling → the inverter/sizing is adequate for the available solar resource in the window under consideration.

7. Operational observability and early warning of deviations. Internal "hourly median" gives a quick indicator when the day is below typical (186 short "deficits") → easy targeting of O&M attention without complex external models.
8. Good data quality. Uniform 5 min resolution (median $\Delta t = 300$ s), consistent channels (P_{dc}, η, PF, Q) → reliable KPIs and robust statistics.
9. Engineering flexibility towards KPI. The profile is ready for direct addition with climate base (PVGIS/PECD/NASA) → quick transition to "official" PR and climate-aligned *curtailment* without reworking the entire pipeline.

All this means lower dispatching and balancing costs thanks to a predictable lunch belt; high compatibility with the grid ($PF \approx 1$, "soft" ramps); efficient resource utilization (no visible system clipping) and clear operational indicators for timely maintenance.

Some practical conclusions and recommendations can be made:

- The profile is operationally robust and compatible with grid practice: no systematic clipping, $PF \approx 1$, moderate ramp-rate values.
- If the aim is an official report ($PR/curtailment$), integrating PVGIS/PECD for the same window will give an absolute "bar" and will turn operational "deficits" into a quantitative loss compared to the potential.
- It is advisable to monitor dynamic tails ($>|5\,\mathrm{kW/min}|$)—although rare, they are markers for "stressful" meteorological events; in future smoothing requirements, these cases are a target for local management.
- TRIP/RESTART are few and short, but correlation with alarm events is useful to confirm that they do not have a common recurring cause.

The indicated KPIs (η, PR, THD/TDD, I_{DC}) are accompanied by 95% confidence intervals (bootstrap by days; metrological contribution by σ_V, σ_I, σ_η and the PQ channel), which allows for correct interpretation of the differences between days/modes.

Validating the capacity against the plate/certificate reduces the uncertainty from the climate scale to δ_C of the order of <1%. This is transferred analogically to PR (exactly $1/(1+\delta_C)$, i.e., $\approx -\delta_C$ for small δ_C) and unilaterally to ΔE via $S_{\Delta E}$ (only when $\hat{P} > P$). In our data, $\delta_C = +0.91\%$ (Table 13), which is less than the measurement uncertainty of some channels and the climate variability in the winter–spring window. Therefore, the contribution of the scale to the total uncertainty of $\frac{PR}{\Delta E}$ is secondary to the meteorological and sensor errors.

Summary: Keep the current inverter settings ($\cos\varphi \approx 1$, no additional smoothing), build a mild climate reference line for daily $PR/curtailment$, monitor dynamic "tails" and rare restarts as signals, and invest efforts in DC health (purity, MPPT balance, shading). This gives the highest return given the already good performance profile shown by the numerical implementation and the resulting performance profile [40,41].

8. Conclusions

This study built a complete "operating profile" of the inverter for the site with a specific location on the territory of the Republic of Bulgaria on 5 min SCADA data (25 January 2025–15 April 2025), using physically based reconstruction of the active power and consecutive statistical and operational analyses. The results confirm a stable and predictable daily course with a clear midday plateau, total production around 12.11 MWh, and an average of $\sim$ 149 kWh/day, without traces of system AC clipping. The load dynamics are "soft", which reduces the need for aggressive smoothing. The power quality is very high, and the inverter efficiency reaches a plateau of ~0.97–0.98 in the nominal zone. The cumulative energy grows smoothly, and the nine TRIP/RESTART events are short and energy-limited. The comparison to the internal hourly median identifies 186 "deficient" segments, which are treated as an operational indicator and not evidence of a grid con-

straint. An external climate base (PVGIS/PECD/NASA) is required for contractual KPIs (PR and climate-aligned curtailment).

The scientific contribution of this study is expressed in the following:

1. Physically informed recovery of P_{AC} from SCADA via P_{dc} and η_{inv}, which avoids numerical instabilities at $|\cos\varphi| \to 1$ and provides a reliable input for all subsequent KPIs.
2. A unified method for inverter profiling at 5 min resolution that combines the following:
   - Diurnal median profile with IQR (robust description of the "typical day");
   - Percentile load indicators (P_{95}, P_{99}, P_{max});
   - Formalized ramp-rate distribution with $|RR|_{95}$ as a grid-relevant KPI;
   - PF/PQ analysis as an injection quality index;
   - $\eta(P)$ curve for estimating conversion losses.
3. An operational referent $\hat{P}_{hour}$ (internal hourly median) and a formal "shortfall" detector, defined as segments $P < 0.6\hat{P}_{hour}$ of minimum duration, which provides an automated "below typical" indicator without external meteorological inputs. A clear distinction is shown between this indicator and the notion of *curtailment*.
4. Climate-friendly production coordination: a two-tier framework for external bases is proposed:
   - Direct PV base (PVGIS, PECD) with stable capacity calibration via percentile scale ($Q_{0.99}$) or robust regression (Huber, no free term);
   - Explanatory base (NASA POWER) via robust regression $P \sim GHI + T + WSP$ with "clean interval" filter rules.

This framework makes it possible to correctly calculate PR (*daily*/*overall*) and climate-consistent *curtailment* $\sum(\hat{P} - P)_+$.

5. Reproducible analytical chain with clearly defined inputs, filters, aggregations and figures (A–K), exported KPI tables, and graphs.
6. A diagnostic matrix for O&M, in which the residuals $r(t) = P - \hat{P}$ can be mapped by hour/temperature/wind for detection of shading, thermal effects, and other issues. This approach links scientific analysis with direct operational actions.

This study has some limitations. The results obtained are valid for the winter–spring window of 25 January–15 April 2025 and are not representative of the summer and autumn seasons. Due to differences in insolation, temperature, day length, and operational modes, it is possible that $\eta(P)$, PR, $|RR|$, clipping probability, and degradation estimates may differ outside the considered window. We will expand the set to $\geq$12 months and include seasonal analysis in a future version (including climate-normalized PR and climate-adjusted curtailment), which will allow for reliable annual generalization.

The accuracy of η and PR is limited by the sum of the accuracies of the DC/AC measurements, the telemetric accuracy of η_{inv}, and the uncertainty of the PQ estimates, all of which are quantified in Section 7 (Table 11).

The added check against the nameplate/certificate and the closure of the formal sensitivity show that the PVGIS $\to$ real power scaling errors are below $\sim$ 1% and have a predictable, directly quantitative effect on PR and ΔE. In conclusion, the combination of physically informed reconstruction, robust statistics, and climate matching offers a methodologically clean and practically efficient approach to inverter profiling. This is directly applicable to daily O&M control and decision-making.

Author Contributions: S.B., I.H., and P.S. were involved in the full process of producing this paper, including the conceptualization, methodology, modeling, validation, visualization, and preparing the manuscript. All authors have read and agreed to the published version of the manuscript.

Funding: This work was supported by the European Regional Development Fund under the "Research Innovation and Digitization for Smart Transformation" program 2021–2027 under Project BG16RFPR002-1.014-0006 of the "National Centre of Excellence Mechatronics and Clean Technologies", and the APC was funded by Project BG16RFPR002-1.014-0006.

Data Availability Statement: The original contributions presented in this study are included in the article. Further inquiries can be directed to the corresponding author.

Acknowledgments: The present research has been carried out under the project BG16RFPR002-1.014-0006 of the "National Centre of Excellence Mechatronics and Clean Technologies", funded by the Operational Programme Science and Education for Smart Growth. The obtained results have been processed and analyzed within the framework of the project BG-RRP-2.004-0005 "Improving the research capacity and quality to achieve international recognition and resilience of TU-Sofia (IDEAS)", funded by the National Recovery and Resilience Plan of the Republic of Bulgaria.

Conflicts of Interest: The authors declare no conflicts of interest.

References

1. *IEEE Std 1547-2018*; IEEE Standard for Interconnection and Interoperability of Distributed Energy Resources with Associated Electric Power Systems Interfaces. IEEE Standards Association: Piscataway, NJ, USA, 2018. [CrossRef]
2. European Commission. Commission Regulation (EU) 2016/631 Establishing a Network Code on Requirements for Grid Connection of Generators (RfG). *Off. J. Eur. Union L* **2016**, *112*, 1–68, (CELEX: 32016R0631). Available online: https://eur-lex.europa.eu/eli/reg/2016/631/oj (accessed on 11 October 2025).
3. *IEEE Std 519-2014*; IEEE Recommended Practice and Requirements for Harmonic Control in Electric Power Systems. IEEE Standards Association: Piscataway, NJ, USA, 2014. [CrossRef]
4. International Electrotechnical Commission. *IEC 61000 3 12: Electromagnetic Compatibility (EMC)—Part 3 12: Limits—Limits for Harmonic Currents Produced by Equipment with Rated Current > 16 A and ≤ 75 A per Phase (Consolidated Version Incl. A1:2021)*; IEC: Geneva, Switzerland, 2011/2021.
5. CENELEC. *EN 50530: Overall Efficiency of Grid Connected Photovoltaic Inverters (Amendment A1:2013)*; CENELEC: Brussels, Belgium, 2013.
6. *IEC 61724-1*; IEC 61724-1: Photovoltaic System Performance—Part 1: Monitoring. International Electrotechnical Commission (IEC): Geneva, Switzerland, 2021.
7. *IEC TS 61724-3*; IEC TS 61724-3: Photovoltaic System Performance—Part 3: Energy Evaluation Method. International Electrotechnical Commission (IEC): Geneva, Switzerland, 2016.
8. Underwriters Laboratories. *UL 1741: Inverters, Converters, Controllers and Interconnection System Equipment for Use with Distributed Energy Resources (incl. Supplement SA)*; UL: Northbrook, IL, USA, 2016.
9. Liserre, M.; Blaabjerg, F.; Hansen, S. Design and control of an LCL-filter-based three-phase active rectifier. *IEEE Trans. Ind. Appl.* **2005**, *41*, 1281–1291. [CrossRef]
10. Peña-Alzola, R.; Liserre, M.; Blaabjerg, F.; Ordóñez, M.; Yang, Y. LCL-filter design for robust active damping in grid-connected converters. *IEEE Trans. Ind. Inform.* **2014**, *10*, 2192–2203. [CrossRef]
11. Teodorescu, R.; Blaabjerg, F.; Liserre, M.; Loh, P.C. Proportional-resonant controllers and filters for grid-connected voltage-source converters. *IEE Proc. Electr. Power Appl.* **2006**, *153*, 750–762. [CrossRef]
12. Ciobotaru, M.; Teodorescu, R.; Blaabjerg, F. A new single-phase PLL structure based on second order generalized integrator. In Proceedings of the 37th IEEE Power Electronics Specialists Conference (PESC 2006), Jeju, Republic of Korea, 18–22 June 2006. [CrossRef]
13. Rodríguez, P.; Luna, A.; Candela, I.; Teodorescu, R.; Blaabjerg, F. Grid synchronization of power converters using multiple second order generalized integrators (MSOGI). In Proceedings of the 34th Annual Conference of the IEEE Industrial Electronics Society (IECON 2008), Orlando, FL, USA, 10–13 November 2008; pp. 755–760. [CrossRef]
14. Golestan, S.; Monfared, M.; Freijedo, F.D.; Guerrero, J.M. Dynamics assessment of advanced single-phase PLL structures. *IEEE Trans. Ind. Electron.* **2013**, *60*, 2167–2177. [CrossRef]
15. King, D.; Gonzalez, S.; Galbraith, G.; Boyson, W. *Performance Model for Grid-Connected Photovoltaic Inverters (SAND2007-5036)*; Sandia National Laboratories: Albuquerque, Mexico, 2007. [CrossRef]
16. Stein, J.S. *Models Used to Assess the Performance of Photovoltaic Systems (SAND2009-8258)*; Sandia National Laboratories: Albuquerque, Mexico, 2009. [CrossRef]
17. PV Performance Modeling Collaborative (PVPMC). Sandia Inverter Model—Modeling Guide. n.d. Available online: https://pvpmc.sandia.gov/modeling-guide/dc-to-ac-conversion/sandia-inverter-model/ (accessed on 29 August 2025).

18. PV Performance Modeling Collaborative (PVPMC). Performance Ratio. n.d. Available online: https://pvpmc.sandia.gov/modeling-guide/5-ac-system-output/pv-performance-metrics/performance-ratio/ (accessed on 29 August 2025).
19. PV Performance Modeling Collaborative (PVPMC). Performance Index. n.d. Available online: https://pvpmc.sandia.gov/modeling-guide/5-ac-system-output/pv-performance-metrics/performance-index/ (accessed on 29 August 2025).
20. Esram, T.; Chapman, P.L. Comparison of photovoltaic array maximum power point tracking techniques. *IEEE Trans. Energy Convers.* **2007**, *22*, 439–449. [CrossRef]
21. Ahmed, J.; Salam, Z. A critical evaluation on maximum power point tracking methods for partial shading in PV systems. *Renew. Sustain. Energy Rev.* **2015**, *47*, 933–953. [CrossRef]
22. Kamarzaman, N.A.; Tan, C.W. A comprehensive review of maximum power point tracking algorithms for photovoltaic systems. *Renew. Sustain. Energy Rev.* **2014**, *37*, 585–598. [CrossRef]
23. Hadji, S.; Gaubert, J.-P.; Krim, F. Real-time genetic algorithms-based MPPT: Study and comparison (theoretical and experimental) with conventional methods. *Energies* **2018**, *11*, 459. [CrossRef]
24. Marcos, J.; Marroyo, L.; Lorenzo, E.; Alvira, D.; Izco, E. Power output fluctuations in large-scale PV plants: One-year observations with one-second resolution and a derived analytic model. *Prog. Photovolt. Res. Appl.* **2011**, *19*, 218–227. [CrossRef]
25. Marcos, J.; Storkël, O.; Marroyo, L.; Garcia, M.; Lorenzo, E. Storage requirements for PV power ramp-rate control. *Sol. Energy* **2014**, *99*, 28–35. [CrossRef]
26. Huld, T.; Müller, R.; Gambardella, A. A new solar radiation database for estimating PV performance in Europe and Africa. *Sol. Energy* **2012**, *86*, 1803–1815. [CrossRef]
27. Gracia Amillo, A.G.; Huld, T.; Müller, R. A new database of global and direct solar radiation using the Eastern Meteosat satellite: Models and validation. *Remote Sens.* **2014**, *6*, 8165–8189. [CrossRef]
28. European Commission, Joint Research Centre (JRC). PVGIS—Photovoltaic Geographical Information System. n.d. Available online: https://re.jrc.ec.europa.eu/pvg_tools/en/ (accessed on 29 August 2025).
29. Huld, T.; Gracia Amillo, A.M. Estimating PV module performance over large geographical regions: The role of irradiance, air temperature, wind speed and solar spectrum. *Energies* **2015**, *8*, 5159–5181. [CrossRef]
30. National Aeronautics and Space Administration (NASA). POWER—Prediction of Worldwide Energy Resources. n.d. Available online: https://power.larc.nasa.gov/ (accessed on 29 August 2025).
31. Sparks, A.H. nasapower: A NASA POWER global meteorology, surface solar energy and climatology data client for R. *J. Open Source Softw.* **2018**, *3*, 1035. [CrossRef]
32. Copernicus Climate Change Service (C3S)/ECMWF. Pan-European Climate Database (PECD) v4.x—Climate and Energy Variables from Reanalysis and Projections [Documentation]. 2025. Available online: https://cds.climate.copernicus.eu/datasets/sis-energy-pecd (accessed on 29 August 2025).
33. ENTSO-E. European Resource Adequacy Assessment (ERAA) 2023—Annex 2: Methodology (v2). ENTSO-E. 2024. Available online: https://www.entsoe.eu/eraa/2023/report/ERAA_2023_Annex_2_Methodology.pdf (accessed on 29 August 2025).
34. Marsh, K. New PECD Version 4.2 Co-Developed with ENTSO-E now Available on the CDS. C3S Announcements. 2025. Available online: https://forum.ecmwf.int/t/new-pecd-version-4-2-co-developed-with-entso-e-now-available-on-the-cds/13497 (accessed on 29 August 2025).
35. IEA PVPS Task 13. *Guidelines for Operation and Maintenance of Photovoltaic Power Plants in Different Climates (Report T13-25:2022)*; International Energy Agency PVPS: Paris, France, 2022.
36. IEA PVPS Task 13. *Uncertainties in Yield Assessments and PV LCOE (Report T13-18:2020)*; International Energy Agency PVPS: Paris, France, 2020.
37. IEA PVPS Task 13. *Performance of New Photovoltaic System Designs*; International Energy Agency PVPS: Paris, France, 2021.
38. IEA PVPS Task 13. *Assessment of Photovoltaic Module Failures in the Field (Report T13-09:2017)*; International Energy Agency PVPS: Paris, France, 2017.
39. IEA PVPS Task 13. *Degradation and Failure Modes in New Photovoltaic Cell and Module Technologies (Report T13-30:2025)*; International Energy Agency PVPS: Paris, France, 2025.
40. Todorov, G.; Kralov, I.; Koprev, I.; Vasilev, H.; Naydenova, I. Coal Share Reduction Options for Power Generation during the Energy Transition: A Bulgarian Perspective. *Energies* **2024**, *17*, 929. [CrossRef]
41. Hinov, N. Smart Energy Systems Based on Next-Generation Power Electronic Devices. *Technologies* **2024**, *12*, 78. [CrossRef]

Disclaimer/Publisher's Note: The statements, opinions and data contained in all publications are solely those of the individual author(s) and contributor(s) and not of MDPI and/or the editor(s). MDPI and/or the editor(s) disclaim responsibility for any injury to people or property resulting from any ideas, methods, instructions or products referred to in the content.